Marine and Petroleum Geology 121 (2020) 104603

Contents lists available at ScienceDirect

Marine and Petroleum Geology

journal homepage: www.elsevier.com/locate/marpetgeo

Research paper

Caprock characterization of Upper Jurassic organic-rich shales using acoustic properties, Norwegian Continental Shelf

Jørgen André Hansen [a,*], Nazmul Haque Mondol [a,b], Filippos Tsikalas [c,a], Jan Inge Faleide [a]

[a] Department of Geosciences, University of Oslo, P.O. Box 1047, Blindern, NO-0316, Oslo, Norway
[b] Norwegian Geotechnical Institute (NGI), P.O. Box 3930, Ullevaal Stadion, NO-0806, Oslo, Norway
[c] Vår Energi AS, P.O. Box 101, Forus, NO-4064, Stavanger, Norway

ARTICLE INFO

Keywords:
Norwegian continental shelf
Caprock
Upper Jurassic shale
Shale composition
TOC
Brittleness
Rock physics

ABSTRACT

Our analysis of a comprehensive well log database and complementary mineralogical and geochemical information indicates that the risk for Upper Jurassic shales on the Norwegian Continental Shelf (NCS) to permit severe leakage of hydrocarbons from the reservoir is generally low, even in the case of substantial uplift. The content of brittle minerals, organic content, and compaction are dominant factors that explain the observed discrepancies in acoustic properties of organic-rich caprock shales. In particular, variations in silt-clay content in clay-dominated shales are found to primarily influence sonic velocity and to correlate closely with gamma-ray where the uranium contribution is limited ("grey shales"). Changes in organic content exhibit a stronger density-component and are seen to counteract or mask the compaction effect on velocity and density in Kimmeridgian black shales. The Hekkingen, Draupne and Tau formations are distinctly different from the underlying grey shale formations in acoustic properties, despite that the latter group also contains significant amounts of organic matter. Based on the low permeability and high capillary sealing capacity of clay-dominated shales, we conclude that even for a silty seal, migration through the caprock matrix is highly unlikely. Furthermore, tectonic fracturing is an ineffective leakage mechanism when the seal is poorly consolidated/cemented prior to uplift. Brittleness, related to both mineralogical composition and consolidation, is consequently a crucial parameter for predicting seal integrity in exhumed basins. Our rock physics framework and interpretations relate this rather qualitative parameter to acoustic properties, and thus, to seismic data.

1. Introduction

A functioning caprock is one of the three vital components conventionally defining a play within the context of an operating petroleum system. Petroleum accumulations form when the hydrocarbon influx into a trap is greater than the outflow, a balance managed by hydrocarbon generation, migration, and caprock sealing capability. Leakage may occur through the caprock matrix if the permeability is sufficiently high, or by tectonic and/or overpressure-driven fracturing (Ingram et al., 1997; Bjørlykke, 2015). Downey (1984) summarized the importance of top seal integrity and highlighted the strong transmissive abilities of (open) fractures. Furthermore, when considering reservoirs and seals for CO_2 sequestration, the difference between a caprock that will retain gas/CO_2 and one that is only capable of trapping oil is of absolute importance.

The most prolific plays on the Norwegian Continental Shelf (NCS; Fig. 1a) rely on Jurassic reservoirs and equivalent age source rock and caprock formations (Hansen et al., 2019, 2020; NPD, 2019). The Norwegian Petroleum Directorate (NPD) states that the presence of a caprock with sufficient sealing capacity, coupled with Cenozoic uplift and associated erosion, gas expansion and possible fault reactivation, are critical factors for the Jurassic plays in the Barents Sea (Fig. 1b). Similarly, in the North Sea (Fig. 1c), Jurassic reservoirs and plays rely on the time-equivalent formations for primary seals as in the Barents Sea. An additional, more restricting consideration for the North Sea region is the limited and localized source rock maturation due to shallow burial in regions close to the present-day Norwegian mainland. A functioning caprock with minimal leakage could consequently be essential to compensate for small generated and expelled hydrocarbon volumes, as late Cenozoic uplift is considered to have de-activated the petroleum system relatively quickly after the onset of oil generation (Ritter, 1988; Hermanrud et al., 1990).

* Corresponding author.
E-mail address: j.a.hansen@geo.uio.no (J.A. Hansen).

https://doi.org/10.1016/j.marpetgeo.2020.104603
Received 31 January 2020; Received in revised form 7 June 2020; Accepted 16 July 2020
Available online 21 July 2020

Our study is motivated by multiple dry wells and technical discoveries in recent years, particularly in the substantially uplifted Barents Sea region, but also by several cases of minor gas or oil shows encountered in the North Sea. Understanding if the hydraulic and capillary integrity of the caprock (as top seal) has been of importance for dry prospects will be of help in future exploration efforts. Furthermore, ultra-shallow discoveries with thin overburden shale sequences, such as the Wisting discovery in the Barents Sea (Hoop area, Fig. 1b), particularly instigate a greater focus on top seal capacity, fracture potential, and exhumation effects. The primary objective of the study is to investigate the elastic properties and related sealing efficiency of important caprock formations on the NCS. In particular, the effects of mineralogical composition, clay-silt-sand proportions and organic content, all related to depositional setting, are investigated at relevant maximum burial and net exhumation, i.e., consolidation states. We utilize petrophysical well log data and rock physics crossplots to compare a wide variety of caprock formations within and across the studied regions. Supplemental information is gathered from XRD (mineralogical) analyses, geochemical analyses, composite logs, completion reports, and seismic data.

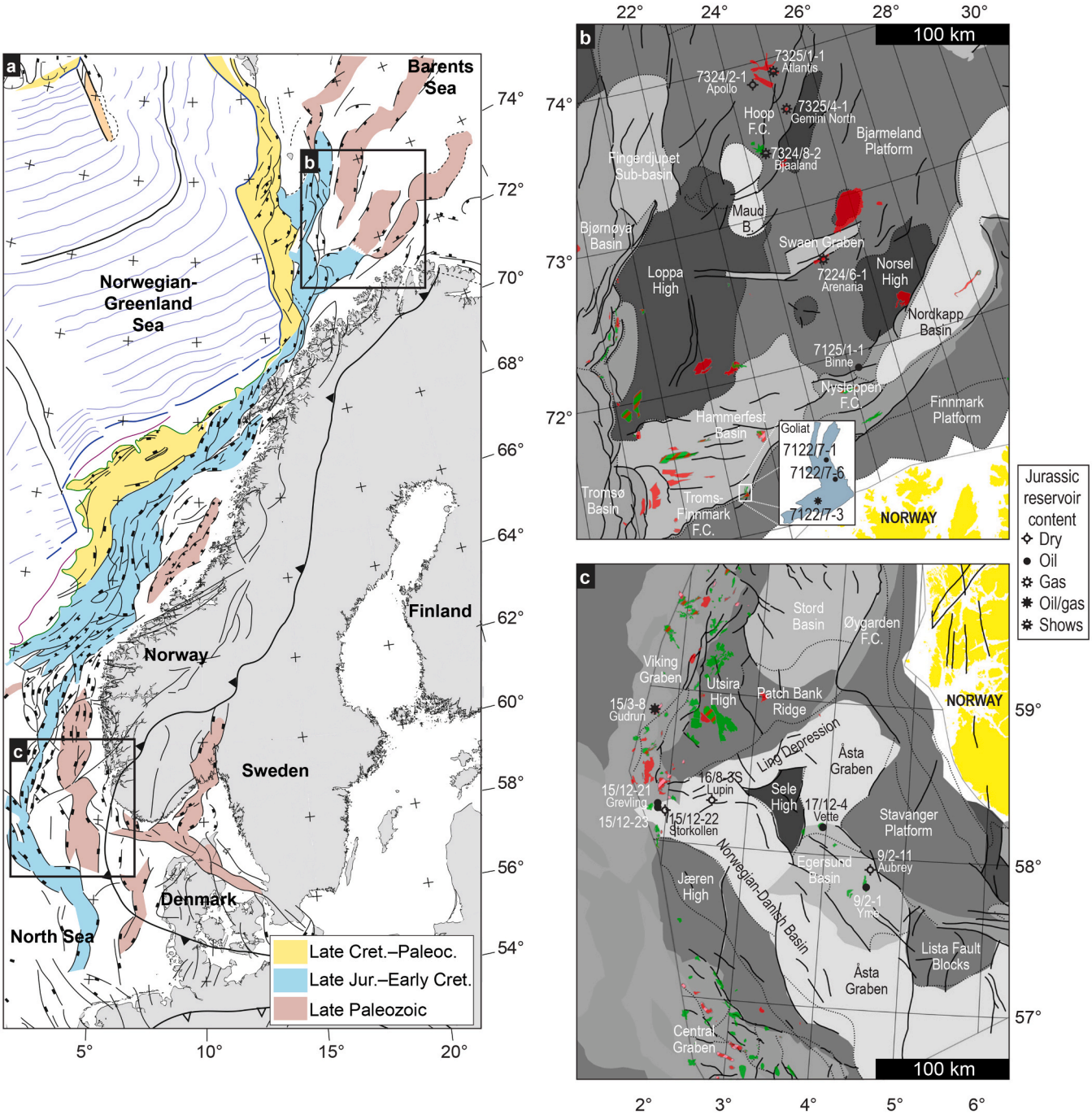

Fig. 1. (a) Structural elements and main faults on the Norwegian Continental Shelf (NCS), and associated timing of rift phases (modified from Faleide et al., 2015). South-western Barents Sea (b) and Central-Northern North Sea (c) overview maps outline structural elements, hydrocarbon fields and discoveries, and wells included in the current study annotated by prospect or field name (adapted from NPD, 2019 FactMaps).

2. Geological setting and lithostratigraphy

Multiple rift episodes preceding continental breakup in the NE Atlantic have largely shaped the structural configuration of all three primary provinces of the NCS (Fig. 1a; e.g., Faleide, et al., 2008, 2015). Both the Barents Sea (Fig. 1b) and the North Sea (Fig. 1c) thus share a series of structural and depositional traits, yet there are many differences, mainly related to the Cretaceous-Cenozoic burial history and exhumation. The Early Cretaceous was dominated by NW-SE oriented rifting, followed by rapid subsidence, siliciclastic deposition, infill and draping of the rift topography. Whereas regional transgression and deposition of thick carbonate sequences characterize the Late Cretaceous in the North Sea, time-equivalent marine deposits on the Barents Shelf are highly condensed due to uplift, erosion, and/or nondeposition in large areas. Cenozoic uplift and erosion affected both the eastern part of the central and northern North Sea and the entire Barents Sea areas. However, the latter has experienced multiple episodes, and an overall higher amount of net erosion, with estimates around 1–1.2 km in the Goliat field area and ~2 km in the Hoop area (Fig. 1b; Henriksen et al., 2011; Baig et al., 2016). The Central North Sea net uplift estimates range from zero to around 0.7 km from the eastern flank of the Viking Graben towards the Stavanger Platform closer to the present mainland (Hansen et al., 2017; Baig et al., 2019).

Fluvial, coastal plain and deltaic deposits to shallow marine sandy facies characterize the Upper Triassic-Middle Jurassic formations, which are the most important and frequent target reservoirs in hydrocarbon fields and discoveries on the NCS (Fig. 2; Vollset and Doré, 1984; Dalland et al., 1988; NPD, 2019). The Upper Jurassic–lowermost Cretaceous Hekkingen, Draupne and Tau formations (Fig. 2) are time-equivalent to the UK Kimmeridge Clay Formation and predominantly consist of organic- and clay-rich black claystone. The underlying Fuglen, Heather and Egersund formations (Fig. 2) are characterized by dark-to-light grey shales with more variable and overall lower organic content (Vollset and Doré, 1984; Dalland et al., 1988; Hansen et al., 2019). The shale formations act as both source rocks and caprocks for the underlying reservoir sandstones. Other than hydrocarbon migration from deeper sections into shallower, predominantly structural traps, there are cases of locally sourced stratigraphic traps such as intra-Draupne and intra-Heather formation sandstones (e.g., 15/3-1S Gudrun and 35/9-7 Skarfjell).

Although the examined Upper Jurassic shale formations represent distinct units, they all relate to deposition in marine environments following widespread rifting and transgression, reflected by a prevalence of fine-grained material (siliciclastic mud, silt, and occasionally carbonate). Thicknesses and lithology can vary greatly between basin axis and margin. One of the main differences between the older (Egersund, Heather and Fuglen) and younger (Tau, Draupne and Hekkingen) shale formations is the amount and quality of organic matter (terrestrial versus marine) that was deposited and preserved. Similarly, the timing, distribution and development of each formation are not exactly the same across the different areas. Generally, the highly radioactive Tau, Draupne and Hekkingen formations are best characterized by deposition in restricted marine environments, with high organic productivity, low circulation and anoxic conditions due to uneven topography following the tectonic movements (Doré et al., 1985; NPD, 2019). There are substantial internal variations in organic content and gamma-ray intensity, which typically increase upwards in the North Sea formations and downwards in the Hekkingen Formation in the Barents Sea. Such

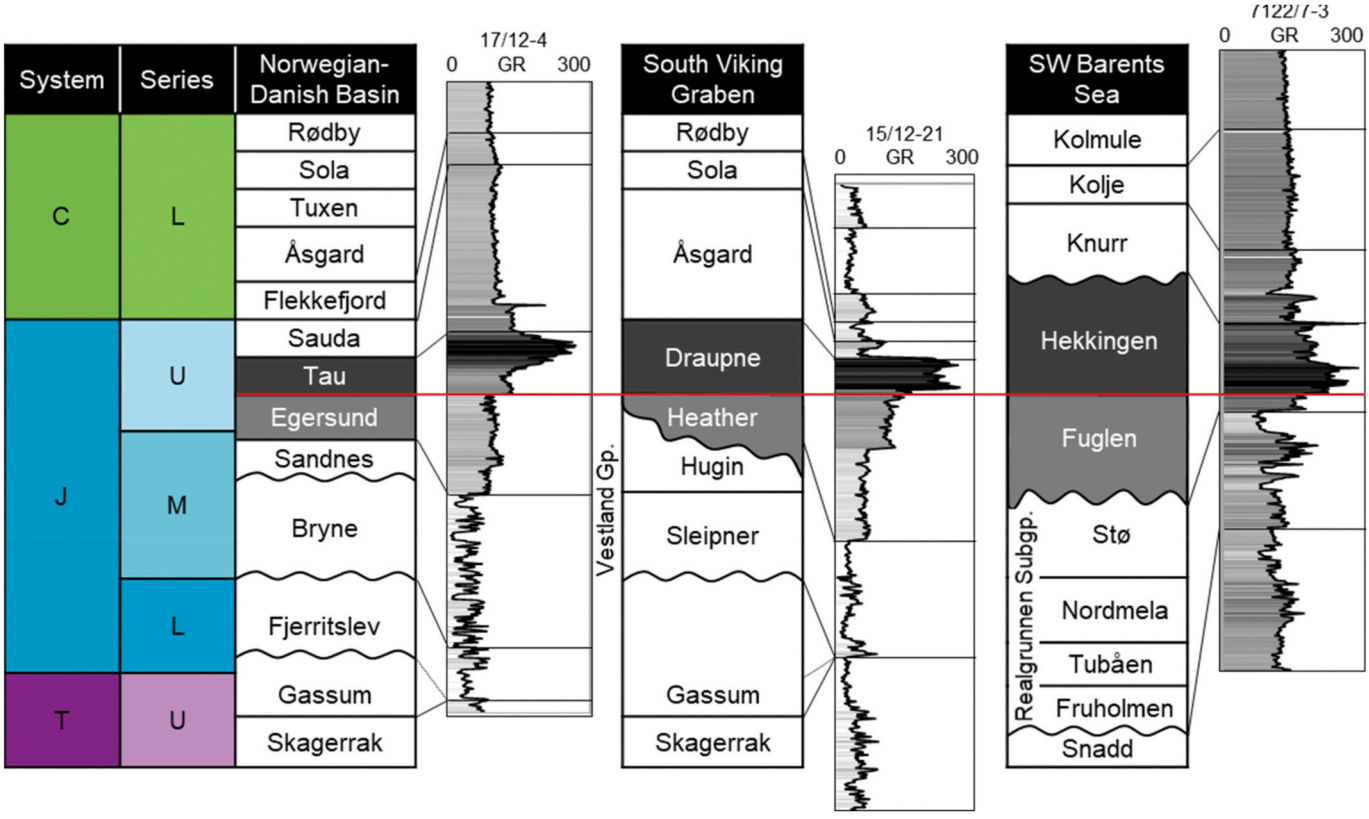

Fig. 2. Lithostratigraphic correlation between roughly age-equivalent formations of the Norwegian North Sea (example wells 17/12–4 in the Norwegian-Danish Basin and 15/12–21 in proximity of the Southern Viking Graben) and the southwestern Barents Sea (represented by well 7122/7–3 in the Goliat field area within the Troms-Finnmark Fault Complex). The gamma-ray (GR) logs have the same vertical scale, and are referenced to the Upper Jurassic formation boundary assigned to the base Kimmeridgian (marked by the red line). Despite the vast distance between the two provinces, we note a characteristic gamma-ray response in the Upper Jurassic shale formations compared to underlying and overlying sequences. Nomenclature after Vollset and Doré (1984), Dalland et al. (1988) and NPD (2019). (For interpretation of the references to color in this figure legend, the reader is referred to the Web version of this article.)

internal variation is the reason for subdividing the Hekkingen Formation into two members identified in certain wells, namely Alge (lower, most organic-rich, black paper shale) and Krill (upper, brownish-grey to dark grey shale). In the earlier rift stage, less prevalent tectonic barriers and consequently more open, but still low-energy marine conditions describe the depositional setting of the Egersund, Heather and Fuglen formations (NPD, 2019).

3. Database and methods

Key information on exploration wells used in this study is summarized in Table 1. All wells contain a standard petrophysical suite of high-quality logs, including logged V_S data in all wells except 7122/7–1 and 9/2–1. The petrophysical well log data were subjected to thorough QC, including removal of spikes and borehole-related artefacts, marking carbonate stringers, and finally used to define representative zones within each well and formation. Seven samples from cores and cuttings were subjected to bulk XRD analysis as a supplement to published data. A high quality, multi-azimuth prestack 3D seismic dataset has been utilized for studying the Goliat field. This dataset was acquired to better illuminate the faulted and complex Goliat reservoir compartments (see Buia et al., 2010; Yenwongfai et al., 2017, 2018 for further details). The mineralogical composition of core samples and cuttings was analyzed in order to justify a comparison between different shale formations deposited in two separate areas of the NCS. Thin sections were prepared from samples to observe the microscale texture and fabric in different levels of the shale and sandstone formations encountered in well 15/12–21 (2905 m, 2929 m, 3030 m and 3057 m). Following QC of wireline logs, shale volume, velocities and other derived elastic properties (AI, V_P/V_S, Poisson's ratio, Young's modulus, Lambda-Mu-Rho [LMR]) were calculated and used to compare a wide variety of Upper Jurassic caprock sections in the North Sea and Barents Sea. For clarity, examples presented in this paper are only expressed in crossplots of V_P versus density, or AI versus V_P/V_S. The seismic dataset was used to understand the geometry and structure of the Goliat field, identify amplitude anomalies (full stack and angle stack data), and compare seismic scale inversion data to rock physics models and trends observed in the well logs.

Table 1
Overview of exploration wells included in the database.

Well (prospect/field)	Net uplift (km)	Content of Jurassic reservoir	Primary seal fm.	Sample/XRD
15/12–21 (Grevling wildcat)	0	Oil	Draupne &	This study
15/12–22 (Storkollen)	0	Dry	Heather	–
15/12–23 (Grevling appr.)	0	Oil		–
15/3–8 (Gudrun)	0	Oil	Draupne	This study
16/8-3S (Lupin)	0	Dry		Zadeh et al. (2017)
17/12–4 (Vette)	0.4	Oil	Tau &	This study
9/2–1 (Yme)	0.5	Oil	Egersund	Kalani et al. (2015)
9/2–11 (Aubrey)	0.6	Dry		–
7122/7–1 (Goliat wildcat)	1.2	Oil	Hekkingen	–
7122/7–3 (Goliat wildcat)	1.2	Oil and gas	& Fuglen	Nooraiepour et al. (2017)
7122/7–6 (Goliat appr.)	1.2	Oil		–
7220/10–1 (Salina)	1.2	Gas		Nooraiepour et al. (2017)
7324/2–1 (Apollo)	2.0	Dry		–
7224/6–1 (Arenaria)	1.4	Low saturation gas		–
7324/8–2 (Bjaaland)	1.8	Dry with shows/fizz gas		–
7325/1-1 (Atlantis)	2.0	Dry with oil shows		–
7325/4–1 (Gemini North)	1.9	Gas		–
7125/1-1 (Binne)	1.3	Oil	Hekkingen	Zadeh et al. (2017)

Note: Net uplift (difference between maximum burial depth and present burial depth) estimates are according to Baig et al. (2016, 2019), based on a composite analysis of Early Cretaceous to Early Miocene shales and Late Cretaceous to Early Paleocene carbonates in the North Sea, and Aptian-Albian to Paleogene shales in the SW Barents Sea.

3.1. Reference rock physics model

In order to conduct our investigation, we need to establish a consistent way to evaluate and compare the shale formations. Strictly speaking, only three independent acoustic properties are available to relate rock properties (e.g., derived from well logs) to seismic attributes, and these are P-wave velocity, S-wave velocity, and bulk density. These parameters can, however, be combined and displayed in different ways (typically in crossplots), and are used to calculate other derived attributes that can better highlight certain geological quantities. Crossplotting porosity or density versus P- or S-velocity is direct and intuitive, and is a proven way to assess composition, sorting and cementation (Avseth et al., 2005). AI–V_P/V_S and $\lambda\rho$–$\mu\rho$ (LMR) crossplot domains are also typical for conventional shale-sand discrimination and excel in terms of fluid sensitivity (Goodway et al., 1997; Ødegaard and Avseth, 2004). A crossplot of Poisson's ratio (ν) versus Young's modulus (E), on the other hand, is potentially more intuitive for evaluating the ductility or brittleness of a rock. These properties are sometimes directly related to mineralogy (e.g., Perez and Marfurt, 2014), and are commonly discussed in the context of hydraulic fracturing of unconventional shale reservoirs (e.g., Vernik, 2016) as well as in geomechanical studies (e.g., Gray et al., 2012). Based on what we know about the Jurassic sedimentary strata on the NCS, rock physics models describing a siliciclastic system should be adequate for our investigation.

A broad array of velocity and density data is displayed in Fig. 3 from multiple wells in the North Sea and the Barents Sea where we have a good understanding of the lithologies and fluids present. Fig. 3a shows all data colored according to shale volume (derived from gamma-ray) in a ρ_b–V_P crossplot, whereas Fig. 3b displays a frequency crossplot of only the shale-dominated rocks ($V_{shale}>0.5$ from petrophysical analysis) in terms of ρ_b–V_P. Shale data dominate the lower part of the plots, where P-wave velocity less than about 2 km/s and bulk densities outside of 1.8–2.7 g/cm^3 are rarely observed at any depth. Generalized rock physics models assuming 25 MPa effective pressure serve as bounds of reference, with brine bulk modulus and density of 3.2 GPa and 1.1 g/cm^3, respectively (Batzle and Wang, 1992). Even though there is no restriction on depth or age, the data-spread is relatively well explained and contained by the theoretical physical bounds of brine-saturated clean sandstone (stiff cases represented by the contact cement and constant cement models; Dvorkin and Nur, 1996; Avseth et al., 2005; Mavko et al., 2009) and a simplified pure clay model (Fig. 3a). When filtering out sand-dominated sections, we see that most of the shaly data plot between the clean sand model and the pure clay model (soft model using Tosaya, 1982 mixed clay moduli; Fig. 3b). The highest frequency of data points coincide with the line representing 50% clay (Dvorkin--Gutierrez silty shale model; Avseth et al., 2005). No significant amount of data falls in the range that could be confused with clean sandstone, i.

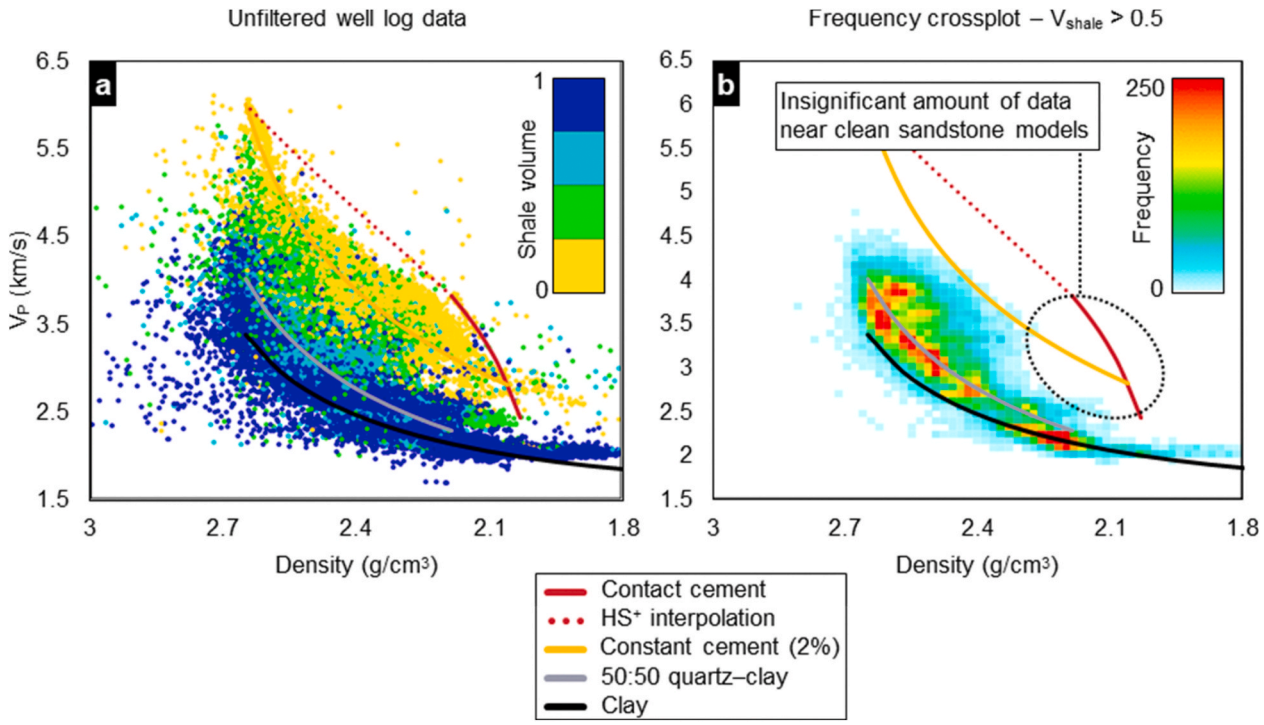

Fig. 3. Crossplots of velocity and density displaying a wide array of data (full vertical range) from wells located in the North Sea and the Barents Sea, only excluding carbonate formations, superimposed on siliciclastic rock physics models. Unfiltered data are color-coded according to shale volume (a). A frequency crossplot (b) showing shale data (V_{shale}>0.5) indicates densely populated areas of the plot as warm colors. The frequency grid is 65 × 65 bins, with number of datapoints within each bin represented by the color scale (minimum 3 points for visualization). (For interpretation of the references to color in this figure legend, the reader is referred to the Web version of this article.)

e., around the contact cement model.

Cementation processes will also consolidate and stiffen clay-dominated lithologies, but no intuitive model accurately describes this behavior in shales due to their complex and variable composition compared to clean sandstone. Therefore, we would generally not expect even pure claystone to follow the black line in Fig. 3 if chemically consolidated. A second consideration is the effect of organic content on shale and sand (kerogen and gas, respectively); explicitly accounting for Total Organic Carbon (TOC) in shales requires more advanced rock physics models (e.g., Guo et al., 2013; Carcione and Avseth, 2015; Zhao et al., 2016). Furthermore, contrasting V_P and V_S relationships will typically indicate fluid anomalies (Hansen et al., 2019). In summary, most of the recorded shale data are relatively well constrained in terms of V_P, V_S (not shown) and bulk density compared to our previous knowledge of siliciclastics. Subsequently, we zoom in on the Jurassic interval to examine how variations in composition, TOC, maximum burial depth (compaction and consolidation) and uplift history manifest in the elastic properties.

4. Results

The following sections concretize the results of our investigation in terms of compiled bulk mineralogy, petrophysical signatures, and rock physics relationships of caprock shale formations. For simplicity and consistency, we focus on crossplots of P-wave velocity versus bulk density when discussing rock physics. The younger, "hot shale" formations (Tau, Draupne and Hekkingen) in all wells in the database display an average V_P of 2.7 ± 0.2 km/s and ρ_b of 2.35 ± 0.12 g/cm^3. The corresponding values for the underlying formations (Egersund, Heather and Fuglen) are V_P of 3.3 ± 0.4 km/s and ρ_b of 2.50 ± 0.07 g/cm^3.

4.1. Bulk mineralogy

The ternary diagram in Fig. 4 summarizes the available XRD mineralogy data pertaining to wells in our study, obtained either in this study or from previously published works (Kalani et al., 2015; Skurtveit et al., 2015; Nooraiepour et al., 2017; Zadeh et al., 2017). The TOC measurements (inset table upper right in Fig. 4), not included in the

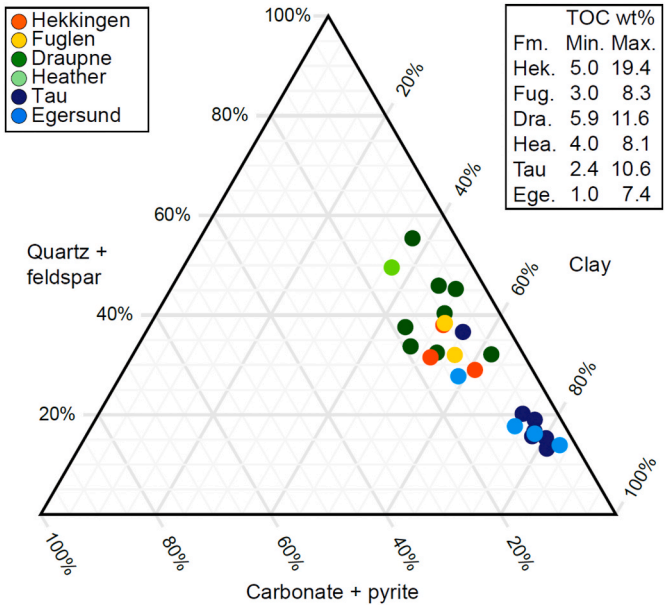

Fig. 4. Ternary diagram showing compiled bulk mineralogy data from this study and literature (Kalani et al., 2015; Skurtveit et al., 2015; Nooraiepour et al., 2017; Zadeh et al., 2017).

compositional fractions, represent the range of organic content observed in the sample database and support the overall impression that the younger formations are more organic-rich compared to the underlying formations. Since there are multiple XRD data sources, some discrepancies between published works are expected but these are assumed irrelevant for the scope of our investigation. These data provide a general range of the mineralogical content (excluding organic matter) of the roughly age-equivalent studied formations in different areas of the NCS. The samples from the Tau and Egersund formations in the Yme area (Fig. 1c) have the highest clay content, constituting more than 70–85% of the bulk volume. The second cluster, formed by the Tau and Egersund samples from the Vette well (17/12–4) along with the Draupne (15/3–8 Gudrun and 16/8-3S Lupin), Fuglen, and Hekkingen (7122/7–3 Goliat, 7120/10-1 Salina, 7125/1-1 Binne) formations contain approximately 45–65% clay and 25–45% quartz and feldspar. Along with the exception of one Draupne sample from the Gudrun well (15/3–8), the Heather Formation sample has the highest Q/F content (50%), consistent with being collected from the lower, silty part of the formation in the Grevling well (15/12–21), but it also has a high TOC content measured to 8 wt%. The content of carbonate and pyrite is subordinate and less variable in all samples (<20%, average around 10%), meaning that the primary differences lie in the balance between silt (Q/F) and clay.

4.2. Lithofacies and composition

Data from the Ling Depression (Fig. 1c) in the North Sea are

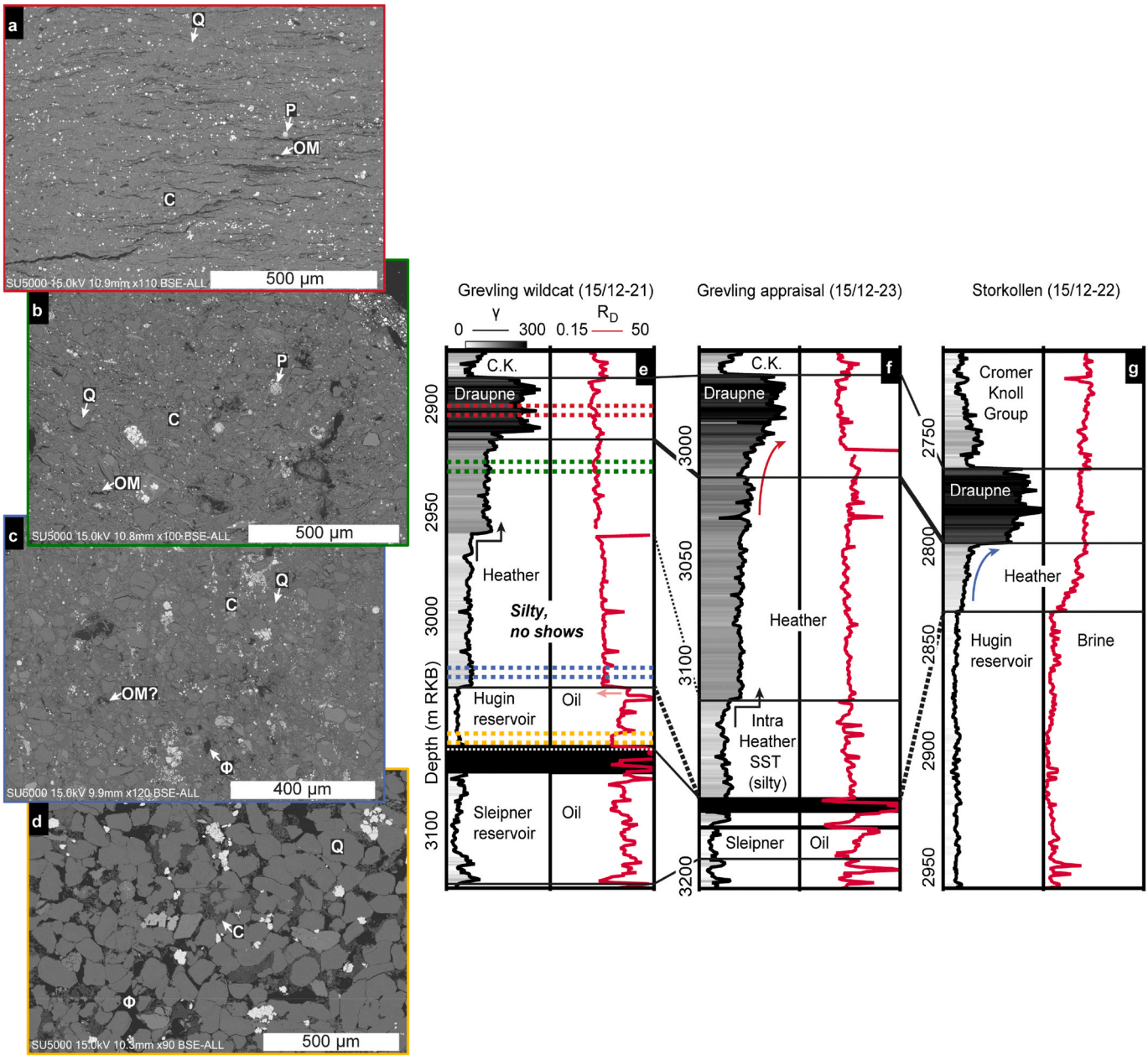

Fig. 5. Micrographs from samples taken in Draupne (a), upper Heather (b), lower Heather (c) and Hugin (d) formations in well 15/12–21 exemplify differences in composition and texture relative to gamma-ray (GR) changes (colors represent ellipses in the crossplot in Fig. 6b). Labels show representative examples of C = clay, OM = organic matter, Q = quartz (some grains consist of feldspar, undifferentiated), P = pyrite, and Φ = porosity. The well log correlation panel (e–g) with three wells from the Grevling area in the southwestern Ling depression (block 15/12; Fig. 1c) displays gamma-ray and deep resistivity (logarithmic scale), and coal layers are marked in black. Dashed lines in Fig. 5e show the sample positions. Although not shown here, velocity and density is missing in the shallow section of well 15/12–21 (<2970 m). (For interpretation of the references to color in this figure legend, the reader is referred to the Web version of this article.)

displayed in Fig. 5, where the Draupne and Heather formations are encountered around 2.75–3.15 km measured depth (MD) below rotary kelly bushing (RKB). Multiple studies have indicated minimal to zero uplift in this area (e.g., Baig et al., 2019 and references therein), meaning that these shale formations are presently at their maximum burial depth. Although the formations approach temperatures associated with the oil window, we do not expect any significant amount of hydrocarbon generation to have occurred that could influence the acoustic properties (Hansen et al., 2019). The wells from the Ling Depression provide a good overview of the range of elastic properties related to composition and texture changes, which are exemplified and supported by samples taken from well 15/12–21 (micrographs in Fig. 5a–d). We can broadly subdivide the caprock section into clay-rich black shale (Draupne Formation, high uranium concentration from spectral gamma ray log), clay-rich grey shale (upper Heather Formation, intermediate uranium concentration), and silty shale (lower Heather Formation) based on the gamma ray log expressions (Fig. 5e–g). It generally appears to be a close relationship between the silt–clay content and texture observed in the different representative micrographs and the gamma ray log. The Draupne Formation sample is clearly dominated by laminated clay and organic matter (OM) with few silt-sized grains (Fig. 5a). The upper part of the Heather Formation is texturally similar, even if the amount of quartz and feldspar grains slightly increase and OM is less dominant (Fig. 5b). Pyrite is also abundant in all shale samples. The intrinsic differences in organic content and depositional conditions (circulation and oxygen) reasonably explain the contrast in gamma-ray between the Heather and Draupne formations. On the other hand, there are significant differences between the microstructure of the fine-grained Hugin Formation reservoir sandstone and the silty lower Heather Formation relative to the change in gamma-ray values. Even if the latter (Fig. 5c) contains a high amount of silt-to sand-sized grains (closer to grain-supported), most of the areas between larger grains are filled with clay, in contrast to the higher porosity of the cleaner sandstone (Fig. 5d).

Crossplots of density versus velocity with the previously described template show separation of formations and wells (Fig. 6a), variation in gamma-ray (Fig. 6b), and uranium from spectral gamma-ray (Fig. 6c). We observe an upwards fining trend in the Heather Formation

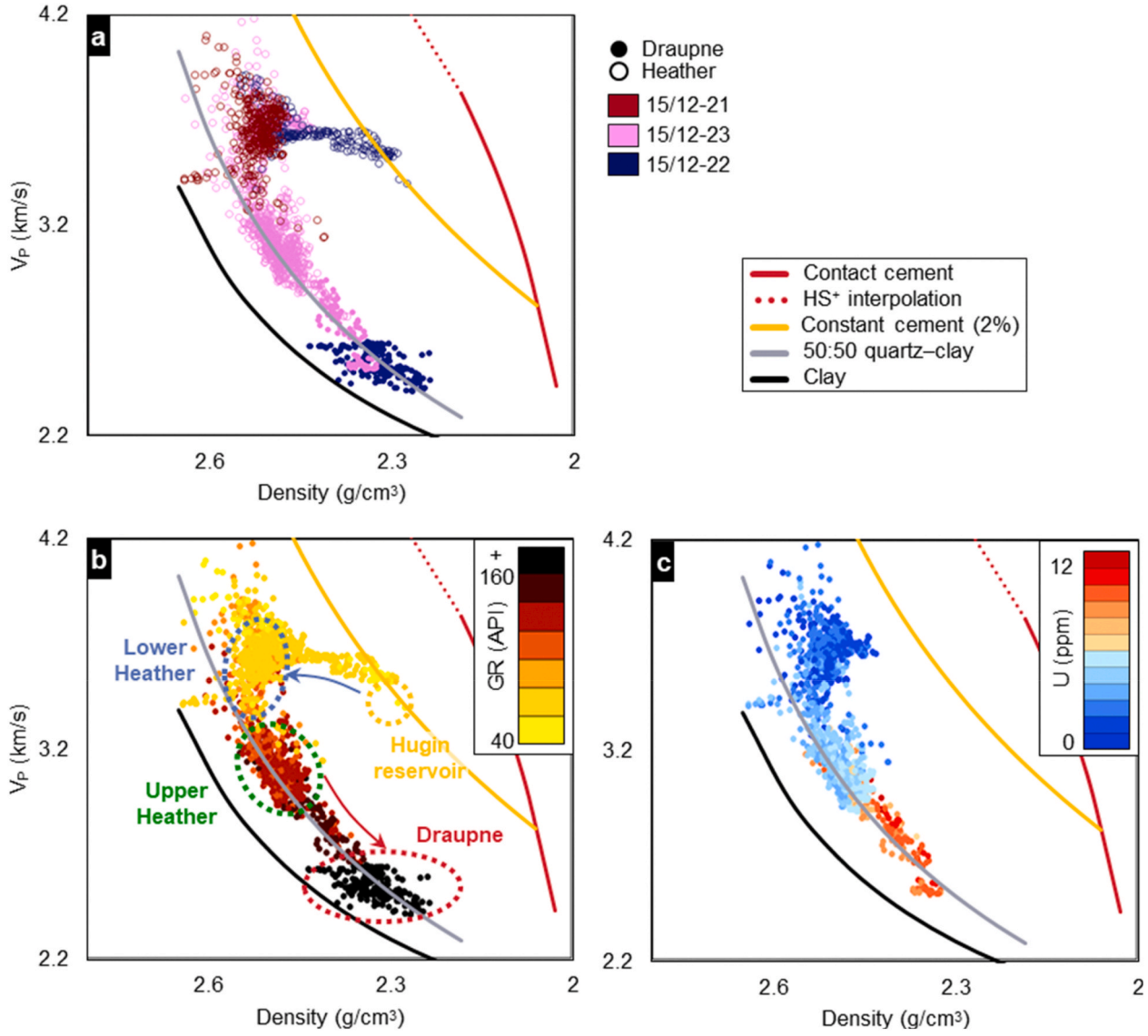

Fig. 6. ρ_b–V_P crossplots corresponding to the three wells from the Grevling area shown in Fig. 5. Crossplot data are color-coded according to well number separated by formation (a), gamma-ray (b), and uranium content from spectral gamma-ray (c); the latter is not recorded in well 15/12–22. Red and blue arrows in the crossplot correspond to fining trends in the gamma-ray log in Fig. 5. (For interpretation of the references to color in this figure legend, the reader is referred to the Web version of this article.)

encountered in the dry Storkollen prospect, and a sharp transition in the Grevling area. The lower part of Heather Formation (well 15/12–22) has similar properties to the underlying clean, highly porous Hugin Formation sandstone, and clearly shifts towards the cemented sand model in Fig. 6b (blue arrow; cf. Fig. 5g). As seen in the lower Heather Formation thin-section (Fig. 5c), however, there is still a prevalent clay fraction compared to the reservoir. The upper and lower Heather Formation sections are clearly separated in the crossplots, predominantly by the lower velocity in the interval with higher gamma-ray log values. An additional increase in gamma-ray from the upper Heather Formation into the Draupne Formation correlates more prominently with decreasing density, but also additionally lowered V_P (red arrow Figs. 5f and 6b). A marked difference is observed in uranium content (Fig. 6c), which signifies more reducing/anoxic depositional conditions (Doveton, 1994; Asquith and Krygowski, 2004), whereas potassium and thorium levels are overall similar. To put this in context, identical behavior and approximately the same range of uranium values are observed between the Hekkingen and Fuglen formations where spectral gamma-ray data are available in Barents Sea wells (7122/7–3, 7122/7–6, 7224/6–1, and 7324/8–2).

In the context of Upper Jurassic shale lithology variations, the Grevling well (15/12–21) encountered a sealing shale on the silty end of the spectrum, as the lower Heather Formation overlies an oil reservoir consisting of the Hugin, Sleipner and Skagerrak formations. No elevated resistivity (~1.8 Ω-m) or oil shows are recorded above the reservoir level, despite the silty top seal (Fig. 5e; NPD, 2019). The resistivity in the oil-saturated sandstone is around 4–5 Ω-m, whereas the sharp spikes correspond to carbonate-cemented layers. Quantitatively, the general risk of leakage as a function of capillary resistance failure, which relates to grain size and pore size variations, can be demonstrated as in Fig. 7. Fig. 7a shows the theoretical realizations of certain capillary and buoyancy forces expressed in MPa. Buoyancy pressure (F_1) is a function of the density difference between the hydrocarbon phase (ρ_{hc}) and water phase (ρ_w), and the hydrocarbon column height (H), expressed as $F_1 = (\rho_w - \rho_{hc}) \times H$. The critical pore throat radius (R), the wetting angle (ϑ), and the interfacial tension (γ) between hydrocarbon and water determine the capillary resistance force (F_2), calculated as $F_2 = (2\ \gamma \cos \vartheta)/R$ (Purcell, 1949). The vertical lines represent capillary resistance pressures, which vary depending on pore throat radius (R), decreasing with increasing clay content and compaction (Schowalter, 1979; Dewhurst et al., 1999). For our calculations, we assume a simplified wetting angle (ϑ) of 0° (water-wet system) and interfacial tension (γ) values of 10 dyn/cm and 40 dyn/cm for oil-water and gas-water, respectively (Schowalter, 1979). Based on observations made by Aplin and Moore (2016), an R-value of 600 nm (6×10^{-5} cm) is a realistic value for a silt-dominated rock (clay fraction around 25%), whereas a very low modal pore throat radius of 10–20 nm ($1–2 \times 10^{-6}$ cm) was found in natural mudstone with clay content around 70%. As demonstrated experimentally by Dewhurst et al. (1999), mechanical compaction does not drastically change these values. Stippled and solid lines in Fig. 7a indicate low and high fluid density contrasts, respectively, using reasonable values of hydrocarbon and brine densities (ρ_{oil} = 0.75–0.85 g/cm^3, ρ_{gas} = 0.25–0.45 g/cm^3 and ρ_{brine} = 1.0–1.1 g/cm^3).

The well completion report of the Grevling well (15/12–21; NPD, 2019) describes the coal layer separating the Hugin and Sleipner formations as a pressure barrier, which limits the effective hydrocarbon column driving the buoyancy force (Hugin Formation hydrocarbon column). Based on drill stem tests the measured oil density (ρ_{oil}) is 0.86 g/cm^3 in the Grevling reservoir, indicating a relatively small contrast between oil and water. Accordingly, the pressure created by the Hugin oil column (dotted line and yellow circle in Fig. 7a) is around the capillary entry pressure associated with silt-dominated caprock. Leakage due to a 28 m column could be possible if the minimum pore throat radii (R) were greater than around 500 nm. A lighter oil phase would increase the likelihood of migration. However, if the clay content is higher and pore throats consequently smaller, the column height and buoyancy would be too low and the capillary entry pressure too high, evident from the vertical lines associated with smaller grain sizes. Fig. 7b makes it evident that a lot of change in capillary integrity occurs in the space between approximate pore throat radii observed for clay-dominated and silt-dominated mudstones (72% and 27% clay, respectively; Aplin and Moore, 2016). When the effective pore throats are less than about 200 nm, the capillary integrity increases exponentially. Hydrocarbons have not been able to migrate/leak into the Heather Formation (similar to Olstad et al., 1997), indicating a sufficiently small modal pore throat size, consistent with the clay matrix-supported texture observed in Fig. 5c. Even when ignoring pressure barriers and including the entire reservoir with an approximate oil column of 130 m, the buoyancy value (F_1) is only approximately 0.2 MPa. This value is still below the capillary resistance of pore throats with a radius of 100 nm, i.e., an order of magnitude larger than the value measured in clay-dominated mudstone. These examples indicate that for hydrocarbon column heights less than ~100 m, even fairly silt-dominated caprocks are very unlikely to leak through the matrix.

4.3. *Range of organic content and burial – an example from the Central North Sea*

Internally in well 9/2–1 (Fig. 8a), the softer section of the Tau Formation with higher gamma-ray and organic content clearly separates

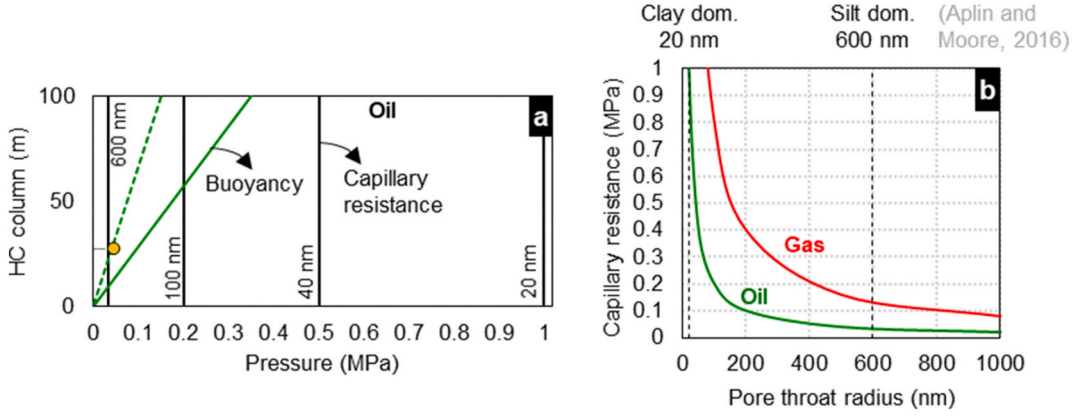

Fig. 7. (a) Buoyancy pressure as a function of hydrocarbon column height in the case of oil. The stippled and solid green lines indicate reasonable values for lower and higher contrast to water, respectively. Vertical lines represent capillary entry pressure/capillary resistance for different effective pore throat sizes (approximate values for silt to clay). (b) Capillary resistance as a function of pore throat radius in the case of oil and gas, which have different interfacial tension. (For interpretation of the references to color in this figure legend, the reader is referred to the Web version of this article.)

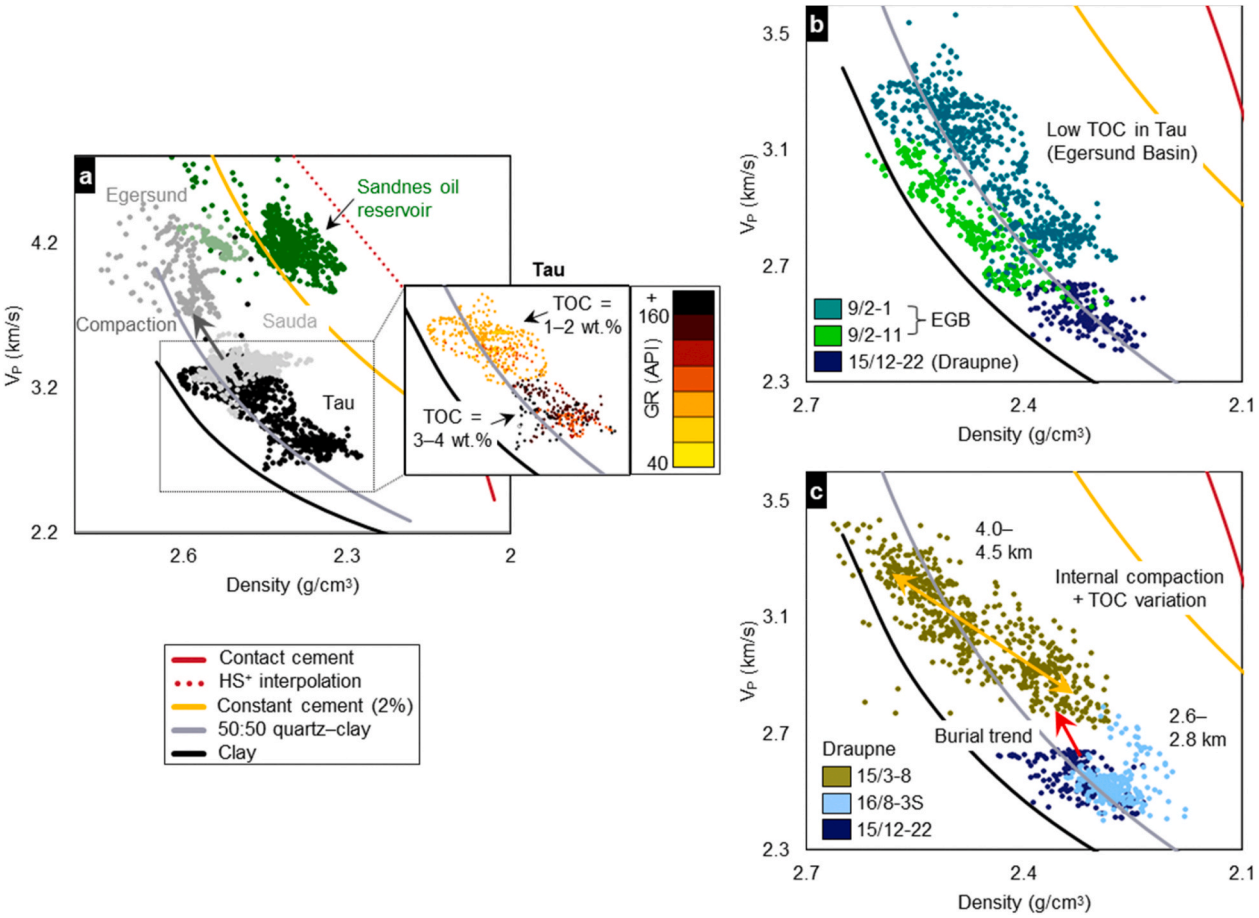

Fig. 8. ρ_b–V_P crossplots highlighting the TOC trends within Tau and Draupne formations considering different maximum burial depths. (a) Examination of internal trends in the Yme well (9/2–1), including surrounding caprock shales and reservoir. (b) Comparison of Tau (Egersund Basin) and Draupne (Ling Depression) formations; note different scale. (c) Deeper buried, oil-mature Draupne Formation as encountered in the Gudrun well (15/3–8) compared to shallower sections in the Lupin (16/8-3S) and Storkollen (15/12–22) wells in the Ling Depression.

from the deeper, low-TOC shale interval (zoomed view in Fig. 8a). The latter is acoustically similar to the younger Sauda Formation, which is typically low in organic content (light grey points). Moreover, the Egersund Formation (heavily filtered from QC) displays values in the upper range of that previously observed in the Fuglen and Heather formations, which is close to the oil sandstone velocity (~4.1 km/s) but higher than the oil sandstone density (~2.4 g/cm^3).

Fig. 8b illustrates how data from the Tau Formation in the Egersund Basin from the Yme (9/2–1) and Aubrey (9/2–11) wells (Fig. 1c), with comparatively lower TOC, plot in relation to the organic-rich Draupne Formation in the Storkollen well (15/12–22; same as Fig. 6). On average, TOC is 2.3–2.7 wt% in the former, whereas the estimate for the latter is 7.1 wt% (Hansen et al., 2019). The Tau Formation in the Aubrey well (9/2–11) has experienced similar burial as the Draupne Formation in the Storkollen well (15/12–22). Regardless of being located on the flank (9/2–11) or central part (9/2–1) of the Egersund Basin, where there is approximately 650 m difference in maximum burial depth over relatively short lateral distance, the Tau Formation data are shifted towards higher velocity and density compared to the Draupne Formation (Fig. 8b). Mineralogical samples from the two respective areas indicate that the Tau Formation should be more clay-rich (Kalani et al., 2015). The acoustic properties do not reflect this difference, as the lower values of velocity and density in the Draupne Formation indicates less brittle and stiff rock. Compared to the rock physics template (cf. Fig. 3), both the Tau and Draupne formations plot around the 50%-clay line, and data from well 9/2–1 (Yme) are shifted towards the sand model compared to well 9/2–11 (Aubrey).

In the Gudrun well (15/3–8) Draupne Formation shale sections (Fig. 8c), we observe very similar acoustic properties to the Tau Formation. Internally, the range of average TOC is 3–6 wt% (Hansen et al., 2019), but the fact that it decreases downwards means that it is difficult to decouple the effect of TOC and compaction in this thick section. Nevertheless, the deepest burial and lowest TOC naturally correlate with the highest velocity and density, and vice versa. Internal variations correspond to an approximate range of V_P and ρ_b of 2.8–3.3 km/s and 2.35–2.6 g/cm^3, respectively. On the other hand, the difference between the shallow, high-TOC section in the Gudrun well (15/3–8) and the Draupne Formation in the Lupin and Storkollen wells (16/8-3S and 15/12–22; Fig. 8c) as a function of 1.0–1.5 km greater burial and onset of oil maturation is minimal (approximate $\Delta V_P = 0.3$ km/s, $\Delta\rho_b = 0.05$ g/cm^3). Synthetic kerogen substitution modelling based on Vernik (2016), assuming a constant mineralogical composition, predicts a similar expression of increasing TOC as observed internally in the aforementioned wells, and interwell trends (cf., Hansen et al., 2019). Testing this method on the Lupin well (16/8-3S) Draupne Formation yields an increase of 0.6 km/s in V_P and 0.15 g/cm^3 in density by perturbing the average TOC from 6.5 wt% to 1.5 wt%.

4.4. *Nuances in sealing capacity – an example from the Goliat field*

The Goliat structure represents a roll-over anticline banked against the Troms-Finnmark Fault Complex in the southwestern Barents Sea (Figs. 1b and 9a; Mulrooney et al., 2017, 2018; Yenwongfai et al., 2017, 2018). The top seal sequence consists of the Fuglen and Hekkingen

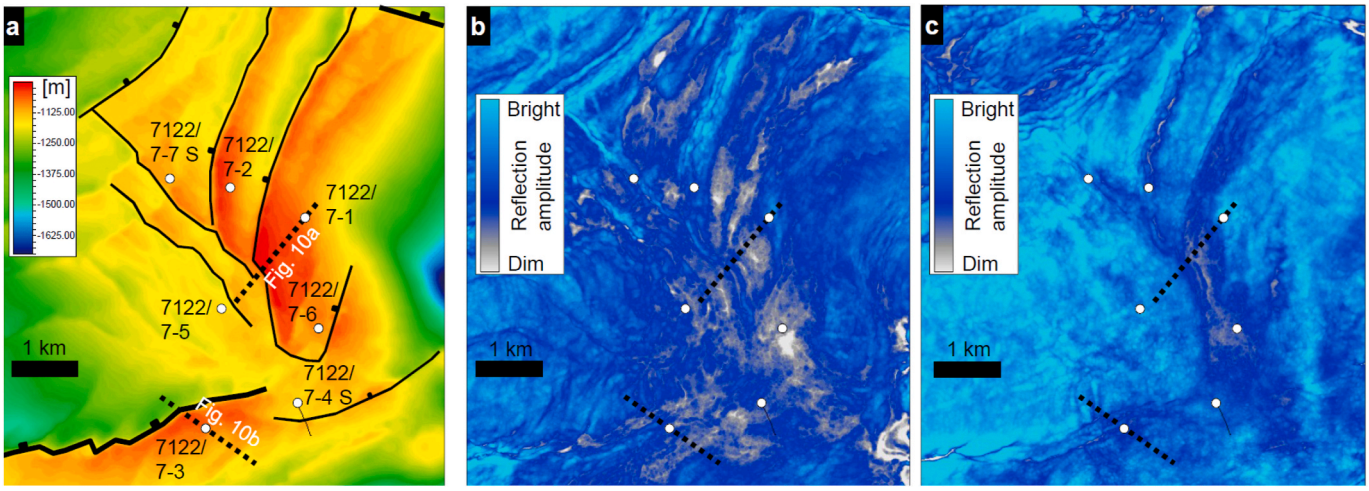

Fig. 9. Goliat field depth-structure map (a) showing the top Realgrunnen Subgroup reservoir level, exploration well locations and dominant faults (cf. Mulrooney et al., 2017 for further detail). Stippled lines indicate locations of cross-sections shown in Fig. 10. Amplitude maps represent the top Hekkingen Formation (b) and top Knurr Formation (c) reflectors.

formations, which again are overlain by Cretaceous sequences. Fig. 9 shows a reservoir depth-structure map (Fig. 9a) and highlights an overburden dim zone along both the top Hekkingen (Fig. 9b) and top Knurr formation (Fig. 9c) reflectors.

Since the Goliat reservoir and caprock retains both oil and gas, we must classify the caprock quality as satisfactory within the scope of petroleum exploration. At the same time, there is evidence in the seismic data of minor differences across the field. In particular, a seismic section across the northern part of the structure (Fig. 10a) highlights a zone of dim amplitudes and distorted reflections above the oil-bearing reservoir, coupled with shallow, bright anomalies. There is distinct dimming of the reflector corresponding to top reservoir level, as well as within and above the overlying caprock shale sequence (Upper Jurassic Hekkingen and Fuglen formations, and Lower Cretaceous Knurr Formation) indicating gas leakage. The dimming does not appear to originate from the fault plane (point source type leakage in cross-section view; Løseth et al., 2009), but appears dispersed above the trap structure which hints towards diffusive leakage or fractured top seal mechanisms.

Signs of dimming, wipeout and leakage are very much reduced in the section near well 7122/7–3 (Fig. 10b). This well encountered gas and oil in the southwestern section of the field (62 m HC column), whereas well 7122/7–6 only contains oil (36 m HC column). These two wells record the caprock properties within and outside the main area of dimming, respectively (Fig. 9a–c). Similarly, well 7122/7-7S confirmed both gas and oil in the Realgrunnen Subgroup level in a segment on the northwestern side of the field outside of the dim zone. There is no oil-water contact (OWC) identified in well 7122/7–3, whereas well 7122/7–6 contains water-bearing Realgrunnen Subgroup sand below the OWC. Similarly, both oil and gas shows were recorded below the OWC in wells 7122/7–1 (38 m oil column) and 7122/7–2 (75 m oil column).

With the seismic observations in mind, the properties of the immediate caprock sequence (Fuglen and Hekkingen formations) above the reservoir in three selected wells are displayed in terms of ρ_b versus V_P (Fig. 10c). The high-porosity end of the clay and 50:50 quartz-clay lines are not directly comparable to these data, but the lower porosity side better reflects the compaction state at the depth of these formations. The Fuglen Formation displays average velocity of around 3.6 km/s and average density around 2.5 g/cm^3. Respective Hekkingen Formation values are 2.7 km/s and 2.2 g/cm^3. Additionally, the Cretaceous Kolmule Formation is included as it represents organic-lean shale, meaning that we can assume the effect of kerogen on the elastic properties to be negligible. This formation was deposited in an open marine setting, appears overall very homogeneous in logs, and contains more clay (68% of bulk volume) than the Hekkingen and Fuglen formations (~55%), and less quartz, feldspar and carbonate (combined ~32% compared to ~45%) judging from XRD data (Nooraiepour et al., 2017). The Kolmule Formation data plot around the pure clay model and display low velocity and density, which is consistent with both the mineralogy and less compaction due to shallower burial depth. The lower, shaly part of the Knurr Formation overlying the Hekkingen Formation is deeper than the Kolmule Formation, and plots around the clay model closer to the Fuglen Formation, which confirms the normal organic-lean shale compaction behavior. By referring to the template, the Fuglen Formation in wells 7122/7–6 and 7122/7–1 appears marginally siltier than in well 7122/7–3, without this being reflected in the gamma-ray. Porosities measured on sidewall cores in well 7122/7–3 range from 6 to 10%, close to what is predicted from the 50:50 quartz-clay model. Similarly, the Hekkingen Formation plots slightly above the 50% clay line, albeit towards much lower velocity and density, removed from the compaction trend. This is coherent with previous indicators of high organic content and deposition in highly restricted marine settings.

4.5. *Regional Barents Sea variations in the Fuglen and Hekkingen formations*

A well correlation panel is shown in Fig. 11a extending from the Goliat field in the south, via the Bjarmeland Platform, and finally through three wells in the Hoop Fault Complex area. The first track shows gamma-ray, whereas the second track shows AI and V_P/V_S. Exhumation magnitude generally increases towards the north in the Barents Sea, corresponding to an increase from approximately 1 km–2 km from left to right in Fig. 11a (Baig et al., 2016). Fig. 11 also displays corresponding ρ_b–V_P crossplots with data from the same wells, colored according to well number (Fig. 11b) and gamma-ray (Fig. 11c). By focusing on the primary seal, i.e., the Fuglen Formation, we can more readily see internal differences in composition and consolidation, over a wide range of net exhumation. We can subdivide the Fuglen Formation into an upper, soft part characterized by high gamma-ray readings, which appears very similar to the Hekkingen Formation, and a lower, stiff part with lower gamma-ray and higher AI values. Only the latter is identified in the Goliat area (7122/7–3), but a distinct upper section is particularly evident in the Arenaria (7224/6–1) and Atlantis (7325/1-1) wells. This is highly similar to the trend observed in the Heather Formation in the North Sea (Figs. 5 and 6). Furthermore, the lithology track included for well 7122/7-3 shows that both the Hekkingen and Fuglen formations were interpreted as clay-dominated but partly silty

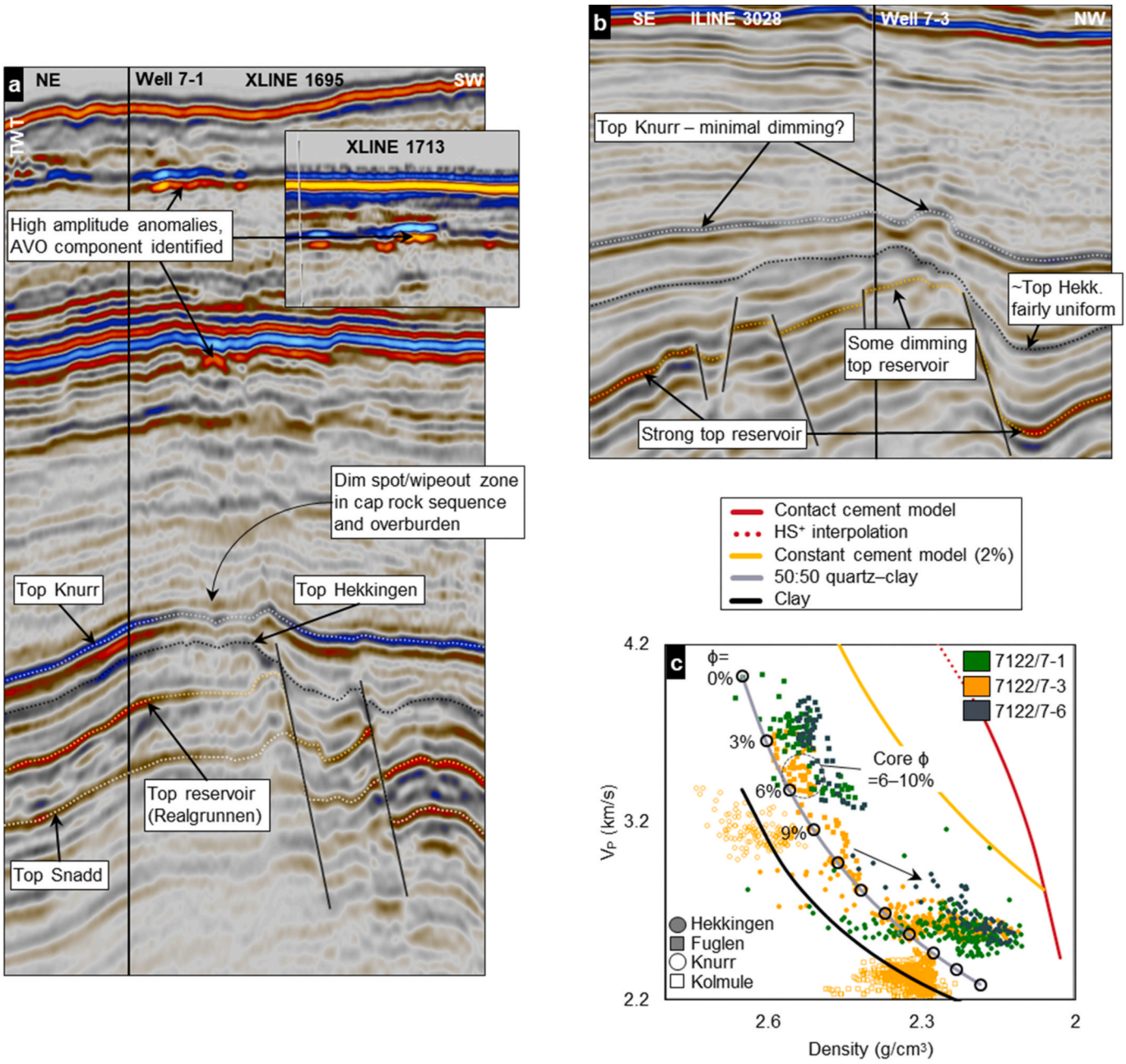

Fig. 10. (a) Goliat field seismic section showing shallow bright anomalies and a dim zone in the caprock sequence and overburden above the trap apex near wells 7122/7–1 and 7122/7–6 (see Fig. 9a for location), which are not prominent in the seismic section near well 7122/7–3 (b). (c) Crossplot showing comparison of the Goliat field caprock inside and outside of the main suspected gas leakage zone (three wells). The black arrow indicates the influence of a higher presence of soft, low-velocity and low-density kerogen in Hekkingen Formation. Data from younger formations in well 7122/7–3 are included for comparison (see Fig. 2 for lithostratigraphy).

(composite log; NPD, 2019), which in conjunction with the XRD data and quartz-clay models imply that Fuglen and Hekkingen formations are overall similar in terms of mineralogy.

The correlation between high velocity and density (i.e., high AI) and low gamma-ray (color code) in the Fuglen Formation is not obvious from the crossplot in Fig. 11c, but AI shows a good inverse correlation with gamma-ray signature internally in each well, which is more readily apparent in Fig. 11a. As the internal separation of yellow, light blue and light grey data points in Fig. 11b shows, there is a change in velocity that drives this sharp drop in AI, rather than a change in density. Note that in the Gemini North well (7325/4–1), we can see a more transitional, upwards decreasing trend in AI rather than the pronounced boundary seen in Arenaria (7224/6–1) and Atlantis (7325/1-1; Fig. 11a). There is little to no change observed in the gamma-ray log (Fig. 11c) or uranium concentration. This gradual change is reflected in the distribution of the Gemini North (7325/4–1) data in Fig. 11b (corresponding red arrow). V_P/V_S ratio is generally higher in the upper, soft part of the formation, as observed for example in the Arenaria well (7224/6–1) where it increases from around 1.9 in the lower section to 2.2–2.3 above the transition.

The trends we have discussed and the associated template naturally transfer to other crossplot domains, e.g., AI–V_P/V_S (as demonstrated in Fig. 12), LMR ($\lambda\rho$–$\mu\rho$) or Poisson's ratio versus Young's modulus (ν–E), although the latter two are not shown herein. Fig. 12 demonstrates how quantities derived from seismic inversion could represent these perceived differences in composition and potential for brittle behavior in terms of AI–V_P/V_S (excluding well 7122/7–1, which does not have

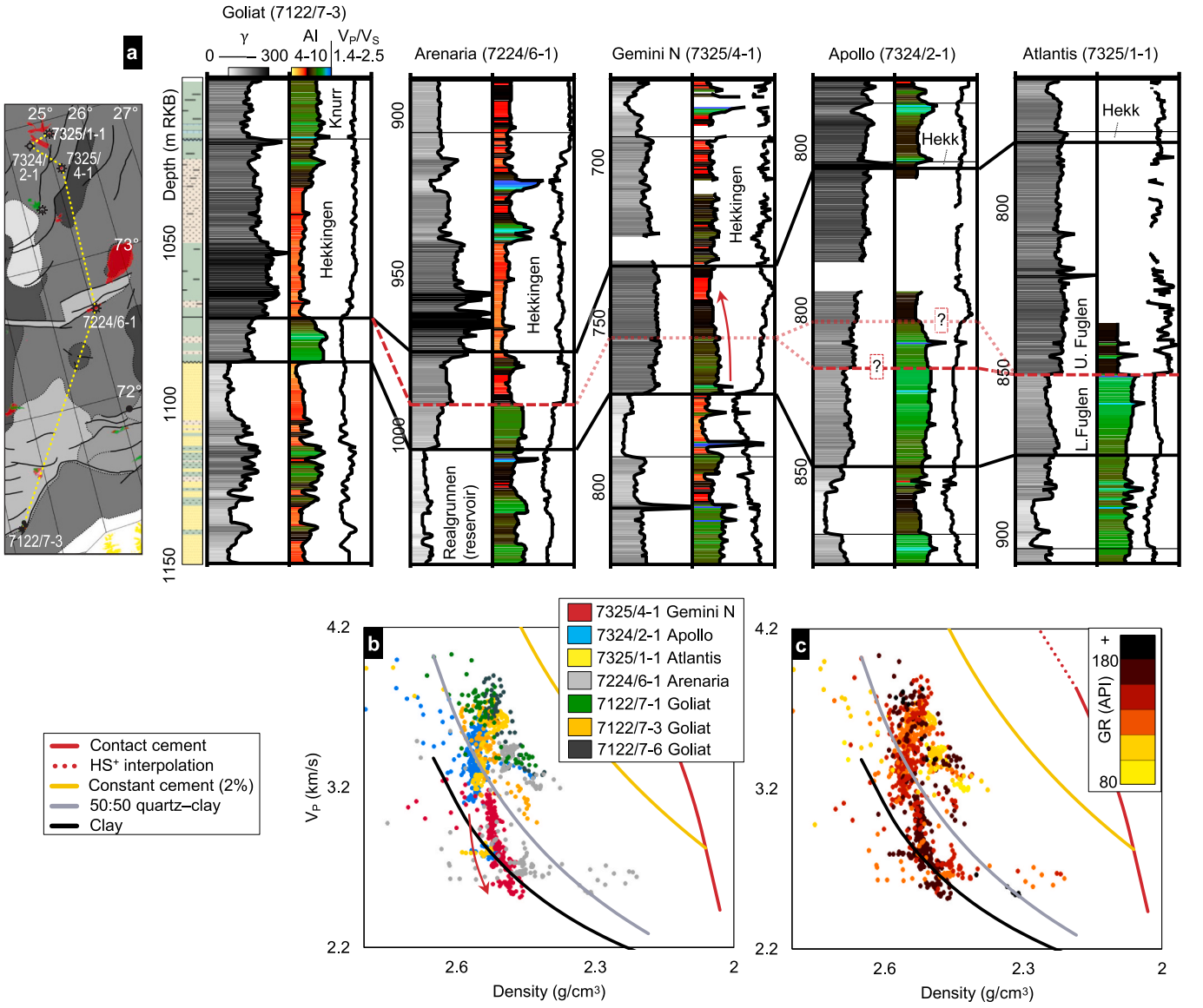

Fig. 11. Barents Sea well correlation panel (a) comparing the Fuglen Formation between the Goliat field in the south to the Hoop Fault Complex area in the north, via the Arenaria well (7224/6–1) located in the Bjarmeland Platform/Swaen Graben (see inset map or Fig. 1b). Corresponding crossplots showing ρ_b versus V_P of the Fuglen Formation are color-coded after well number (b) and gamma-ray response (c). (For interpretation of the references to color in this figure legend, the reader is referred to the Web version of this article.)

measured V_S data). Domains where shear-velocity data are incorporated actually further emphasize the separation between the Fuglen Formation in the Goliat wells (stiff) and wells located further north (Fig. 12a and b; cf. Fig. 11b). The lowermost section of the Hekkingen Formation, often characterized by extremely high gamma-ray and TOC values (herein informally assumed equivalent to the Alge Member), display only marginally lower AI compared to the upper section (Krill Member). However, we observe very low V_P/V_S in some of the data, similar to observations made previously in data from the Tau and Draupne formations in the North Sea (Hansen et al., 2019). As evident from comparing Fig. 12a and b with Fig. 12c, which shows sandstones with different fluid content encountered in these wells, there are two potential areas of overlap between Upper Jurassic shales (Fig. 12a and b) and brine sands, oil sands, or even gas sands (Fig. 12c). The first is the aforementioned lower Hekkingen Formation, and the second is the siltier, more brittle Fuglen Formation interval (Fig. 12b). Finally, data extracted from a small area around well 7122/7-3 based on AVO inversion for P- and S-impedance are displayed in Fig. 12d. The utilized window captures the immediate caprock above the reservoir. Note a tendency of the seismic data falling towards the brittle models rather than the clay models, partially similar to what is observed in Fig. 12a and b, as well as a clear depth trend.

5. Discussion

It has been suggested that the three main factors that may compromise or diminish seal capacity in exhumed basins are seal brittleness, hydraulic fracturing, and diffusion (Doré et al., 2002). The permeability (related to porosity) and pore geometry of sedimentary rocks are largely dependent on the amount of sand- and silt-sized grains compared to clay particles, as well as the compaction state (loading-unloading-reloading history). For a consolidated and uplifted siliciclastic rock, an increasing amount of brittle minerals such as quartz, feldspar and carbonate will also contribute to the potential for brittle fractures in that rock (Gabrielsen and Kløvjan, 1997). Consequently, it is of great value being able to determine whether a caprock is clay-dominated or quartz-rich, because it helps predict whether the seal is more or less prone to fractures (e.g., uplifted regions) and may indicate the potential for leakage in the event

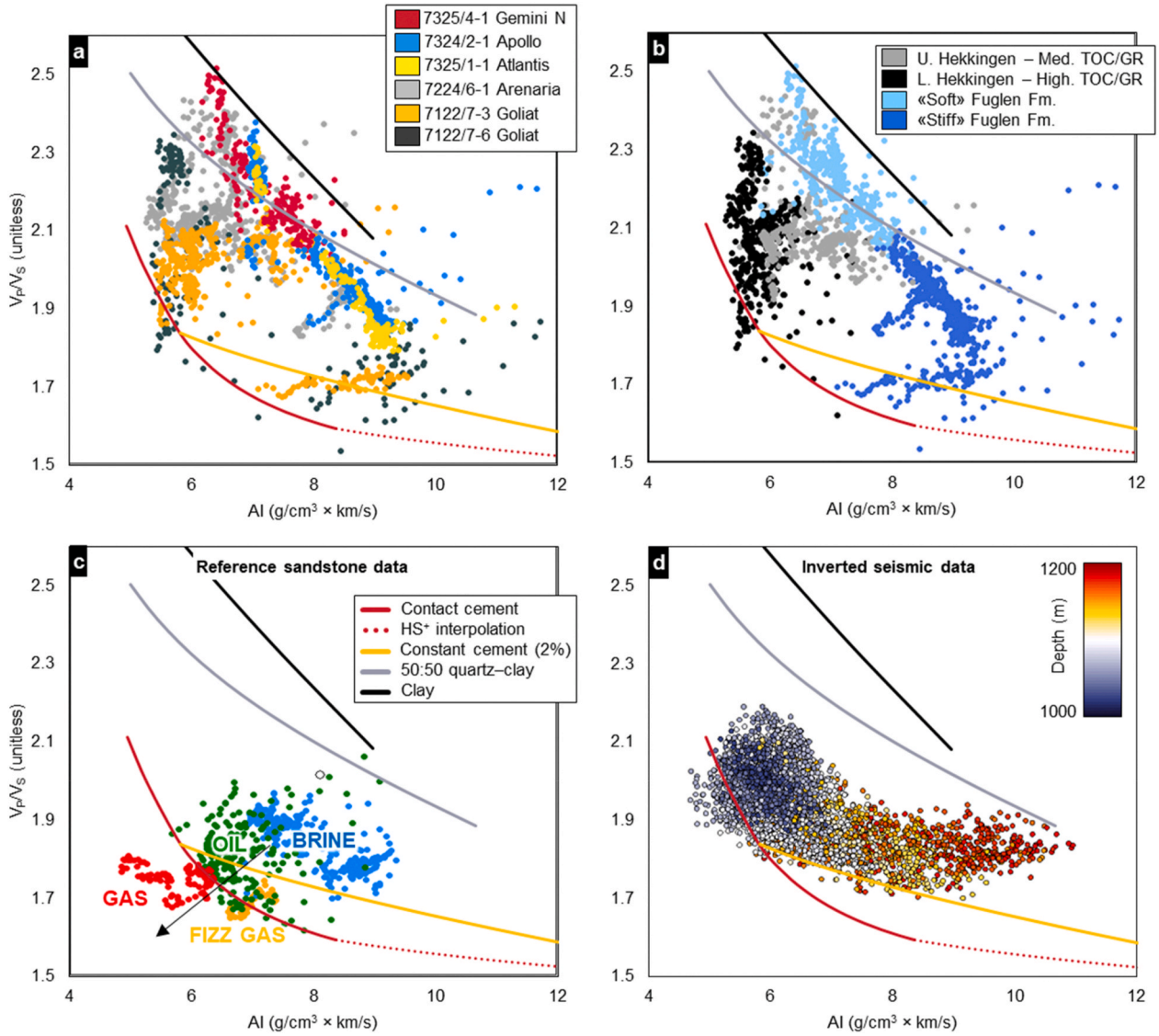

Fig. 12. Rock physics template superimposed on well log data from the Fuglen and Hekkingen formations (cf. Fig. 11b) in the AI–V_P/V_S domain, color-coded after well number (a) and formation sections (b). Sandstone data shown for reference have colors according to different fluid content (c). Seismic inversion data (d) for a window of 10 m above the top reservoir around well 7122/7–3 (±50 IL and XL, increment of 2), roughly represents the expression of the Fuglen Formation. (For interpretation of the references to color in this figure legend, the reader is referred to the Web version of this article.)

of considerable hydrocarbon column heights.

5.1. *Effects of composition and organic content on sealing capacity*

A caprock can act as a capillary seal, implying that no vertical migration takes place unless the buoyancy pressure (pressure in the petroleum phase) exceeds the capillary entry pressure. If the caprock is fine-grained, pore throat radii are small, the capillary resistance is high, and thus a trap can support a larger hydrocarbon column without leaking. A caprock can also act as a permeable flow barrier, which indicates slow leakage through the caprock by Darcy flow or diffusion (matrix-controlled flow; Ingram et al., 1997; Bjørlykke, 2015). Such flow typically relates to light hydrocarbons such as gas (Ingram et al., 1997). Conversely, Teige et al. (2005) have shown experimentally that water may rather flow through a water-wet seal while the capillary forces retain oil. Clay minerals typically dominate the Upper Jurassic caprock composition, and previous studies dictate that the permeability of such fine-grained rocks is generally far too low to allow significant migration of oil through the matrix (Olstad et al., 1997; Bjørlykke, 2015).

We observe that the high organic content in the hot shale formations masks the increase in velocity and density we typical expect from deeper burial and consolidation, when comparing to younger shale formations (e.g., Kolmule shale in Fig. 10c, Sauda shale in Fig. 8a). This is not the case for the three older formations, even though they typically contain substantial amounts of organic matter. Comparing rock sample information with elastic and petrophysical properties reveals that the apparent differences in silt-clay content between age-equivalent formations (e.g., Tau versus Hekkingen) – and conversely, the similarities in composition between older and younger formations (e.g., Fuglen versus Hekkingen) – are fairly discrete (Figs. 6, 8 and 10). Instead, it is apparent that the age-equivalent formations are acoustically similar, and that higher AI and lower V_P/V_S distinguish the older, lower-TOC group. Data from the Tau Formation in the Yme area (Fig. 8a) are a good example, where the TOC is relatively low, but the elastic properties are closer to the organic-rich Draupne Formation (Fig. 8b) than a (sampled) high-TOC Fuglen Formation (Fig. 10c). An important consideration is that gamma-ray values are not directly representative of clay content in a black, organic-rich shale like the Draupne Formation (Fig. 5). As observed in XRD sample data, the mineralogy of the older, less organic-rich formations are typically very similar to the younger,

uranium-rich (Fig. 6c) formations characterized by deposition in a very restricted marine setting. Gamma-ray logs exceeding a certain value do not correlate well with the rock physics models (Draupne versus upper Heather formations; Fig. 6), but clearly correlate with the finer and coarser parts of the Heather Formation. By combined consideration of trends observed in Fig. 8 and the behavior of the other age-equivalent formation pairs (cf. Hekkingen versus Fuglen and Draupne versus Heather) in conjunction with the rock physics model, we suggest that higher TOC explains why a Draupne Formation with similar quartz content can appear less stiff and brittle. TOC is apparently more influential than differences in maximum burial (>1 km difference) on the acoustic expression, as demonstrated by comparisons in Fig. 8.

Consequently, for predicting what the acoustic properties of a given caprock signify, our data suggest that an increase in clay content appears to influence mainly the velocity, as observed internally in the Heather and Fuglen formations (Figs. 6b and 11b). Although the organic content in these older shales is nowhere near negligible, there are clear and consistent differences when comparing to the younger, black, organic-rich Jurassic shale sequence stemming from even more restricted depositional conditions with higher average TOC (Fig. 4). This separation more dominantly manifests in the bulk density values, which are markedly low regardless of the consolidation and maturation state of the shale being examined. The distinction between P-impedance and the separate changes in ρ_b and V_P could be relevant for instance when considering modern wide-azimuth seismic data where information from angles >30° provide better constraints on the density term (in three-term AVO). In turn, this means that with high-quality data, it is feasible to decouple the velocity and density contributions to the acoustic impedance, and per the observations in this paper be able to discern changes in TOC versus mineralogy more clearly. We note that plotting quantities more readily related to conventional prestack seismic data (e.g., AI-V_P/V_S) yield similar trends (Fig. 12), but none of these quantities correlate well with only compaction, organic content or mineralogical composition.

The effect of seal composition is further manifested in the capillary sealing calculations (Fig. 7). In prediction of capillary retention capacity, gas values are poorly constrained compared to oil in terms of both density and interfacial tension, which are crucial to these calculations. In a gas-water system, the buoyancy would be higher because of low hydrocarbon density, but the capillary resistance would also increase due to higher interfacial tension (Bjørlykke, 2015). It is consequently difficult to generalize whether gas is more or less likely to leak from the same reservoir with the same caprock. However, our calculations and evidence from the North Sea indicate that due to the overall high clay content in Upper Jurassic formations, we should not expect the marginal difference in the Goliat caprock composition indicated by the velocity and density in Fig. 10c to explain a change in retention capacity (postulated from seismic hints of gas leakage). Based on rock samples the Fuglen Formation is characterized by similar or higher clay content than the Heather Formation, which is the key factor deciding capillary properties.

5.2. How composition and compaction influence fracture potential and behavior during uplift

The other relevant influence of caprock composition, i.e., minerals and organic content, relates to deformation properties such as brittleness and fracture potential. The approach we present does not directly attempt to quantify brittleness in the sense of brittle deformation as defined in geomechanics (see e.g., Holt et al., 2015 for discussion on this matter), but rather tie factors that facilitate a higher or lower potential for brittle fracturing, predominantly focusing on the rock composition and consolidation. Clay-rich shales have low permeability that may inhibit expulsion of water during compaction (e.g., if burial and sedimentation rates are high), and are therefore prone to overpressure build-up (Hall et al., 1997; Bjørlykke, 2015). The maturity state of organic-rich caprock shales is also important, since generation of liquid hydrocarbon from solid kerogen can cause overpressure and fracturing in tight shales (Kalani et al., 2015). Tectonic fracturing, on the other hand, typically relates to uplift and stress-release in brittle rocks, a factor that in turn primarily relies on the degree of consolidation and stiffening (e.g., through deeper burial and degree of cementation).

No natural seals are perfect, but we see strong indications of non-fault-driven leakage in the caprock and overburden over parts of the Goliat field where there is no gas cap, but where there are hydrocarbon shows beneath the OWC (see Fig. 10a compared to models presented in Løseth et al., 2009). Ohm et al. (2008) proposed that a siltier top seal is more likely to leak gas (compared to the Hammerfest Basin center), and could provide an explanation for the Goliat oil accumulations, i.e., a type II–III trap (Sales, 1993). Leakage of gas allows oil that would otherwise spill to remain in the reservoir during uplift and release of gas from the oil-phase (Lerch et al., 2016). Based on well and seismic data the Goliat structure is underfilled (Tsikalas et al., 2017). Provided that adequate migrated hydrocarbons are available, it appears that the larger structural capacity of Goliat compared to the capillary sealing capacity of a relatively clay-rich rock, is related to a leakage process that must have been aided by fracturing to be effective. Compared to the same shale succession farther north, the gas-retaining Goliat primary top seal (Fuglen Formation) is more brittle/stiff in terms of elastic properties (Fig. 10b; possibly driven by silt content). The reason may be either that the Goliat wells encounter a condensed section, or that the younger, soft Fuglen Formation sequence observed farther north was not deposited in this more proximal area. A softer signature can be explained by a more dominant clay-fraction (soft mineral composition), and/or a higher amount of organic content, both of which are determined by changes in the depositional setting (Doré et al., 1985). Either of these two factors could explain the elevated gamma-ray readings, but as the main change occurs in V_P rather than density, it appears to be driven by mineralogy. If considering the individual caprock quality of the Fuglen Formation, a soft and likely more clay-rich shale overlying the more brittle and stiff lower shale will clearly raise the potential sealing capacity. The former will be less prone to fracturing as well as potentially having lower permeability. Different degrees of microcrystalline quartz cementation sourced from thermal alteration of smectite to illite could be an alternative explanation, which in initial stages correlate with rapid velocity increase, but only small changes in density (Thyberg et al., 2009). Although exhumation estimates carry a lot of uncertainty, maximum burial depth was greater in the Hoop area (~2.2 km below sea floor) than in the Goliat area (~1.9 km below sea floor), which we believe makes cementation a less likely explanation. Since the cementation process is also governed by the time spent in the chemical compaction domain, the timing of uplift phases must be constrained to fully understand its impact, but the interpretation of less fracture-prone cap rock in the Hoop area compared to the Goliat area would remain unchanged.

In a recent study of Barents Sea formations and onshore equivalents, Birchall et al. (2018) have identified underpressured reservoirs both onshore Svalbard and in the Barents Sea, including wells located in the Hoop Fault Complex and Fingerdjupet Sub-basin (Fig. 1b). Following the suspected causes of underpressure – exhumation and associated decompaction – the fact that pressure has not been equilibrated can indicate well-sealed structures with a lack of open fractures (hydraulic or tectonic) to aid flow. On the contrary, based on a numerical rock mechanical model study, Makurat et al. (1992) proposed that more than 1.6–1.7 km of uplift would cause conductive tectonic fractures in the Jurassic caprock interval. However, a substantial gas column was recently encountered in a Jurassic reservoir in the Gemini North well (7325/4–1), with no visible sign of leakage in the caprock formations. Furthermore, in the same well there is no change in resistivity compared to nearby dry wells, and no seismic anomaly (Faleide et al., 2019) as seen over the Goliat field. Fracturing, a suspected product of uplift/unloading, was consequently not pervasive enough to result in seal failure, possibly as a result of relatively ductile shale behavior. The

Makurat et al. (1992) estimate of uplift magnitude required to drive fracturing may consequently be too conservative when more closely considering the geological setting and the very shallow present burial in the Hoop area. Considering an uplift magnitude of 1.9–2.0 km (Løseth et al., 1992; Baig et al., 2016) and a present burial depth of around 0.2–0.4 km below seafloor (BSF) as locally in the wells (Fig. 1b), the caprock and overburden shales may still be relatively unconsolidated depending on the extent of chemical compaction and cementation. In such a scenario, the shale may plausibly have been able to endure the stress-release caused by uplift and unroofing without brittle deformation, i.e., tectonic fracturing. As increasing exhumation and over-consolidation typically relates to more brittle behavior, the trend we observe is the inverse of general expectations. However, the deciding factors for brittleness are maximum burial depth, consolidation, and cementation, or lack thereof, not exhumation magnitude itself. Differences in caprock composition and compaction as seen in Fig. 11 will alter the rock behavior during uplift, and we can speculate that if the uplift in the two areas was equal, the Goliat section would have been more prone to fracturing. As gas discoveries are typically not economically viable in the Barents Sea, partially leaking traps could be positive for oil retention under certain circumstances (Ohm et al., 2008).

As noted, similar shales subjected to roughly the same maximum burial depths, but significantly different uplift (0–2 km) generally exhibit a very similar range of elastic properties (e.g., Figs. 8, 10c and 11b-c). Assuming a relatively equal lithological starting point, as per XRD, gamma-ray log signature and lithological description (Dalland et al., 1988), there is no reason to suspect that the uplifted shales currently contain any higher amount of conductive fractures (e.g., Gabrielsen and Kløvjan, 1997). We would expect that open fractures could potentially have an influence on the porosity and tortuosity and thereby on sonic, density and resistivity logs, if they were indeed "open" and of sufficient intensity. However, the fact that hydraulic fractures can open and close in a valve-like fashion according to episodic pressure build-up makes them inherently hard to identify remotely. Gabrielsen and Kløvjan (1997) presented evidence of fractures in Fuglen and Hekkingen formations from burial and uplift, but also that the fracture frequency is low and the associated risk for hydrocarbon leakage is minor. Even when the shales are extracted from the subsurface in cores, identifying, sorting and understanding in-situ versus drilling- or coring-related fractures in shales is an elaborate process (Gabrielsen and Kløvjan, 1997). In settings where shales have experienced burial and temperatures corresponding to oil maturity, kerogen accumulations could potentially create a type of network during cracking and generation of liquid hydrocarbon from solid organic matter because of sufficiently high OM concentrations, and/or due to fractures driven by overpressure in smaller pods of organic matter. In turn, the wetting phase of this network will be oil, even after expulsion of the generated hydrocarbons, and therefore hydrocarbon from the capped reservoir will more easily be able to migrate through this source/caprock than through the water-wet pore space of an immature shale. There are sections in the Gudrun well (15/3–8) where brine sandstone overlies low-TOC, shaly Draupne Formation sections, which possibly indicates that such fracture networks require a substantial organic matter volume to be influential. Fractures and cracks are not accounted for in the rock physics models we utilized, but an alternative approach that may help identify sections the velocities may be affected in that manner could involve using inclusion-based models that parameterize these processes (e.g., Bredesen et al., 2019).

5.3. Applications in exploration

Firstly, the proposed framework can be used to predict caprock behavior and causes of leakage. Fig. 13a summarizes schematically the trends we can generalize based on our database. As an example of comparing data with the template, we plot a thin Bjaaland (7324/8–2) prospect seal (dry well/fizz gas) encountered in a well close to the Wisting (7324/8–1) discovery (Fig. 13b). This caprock section has a soft (clay-rich) signature, appears to be less silty, less brittle and consequently less fracture-prone than for instance the Goliat caprock, which plotted around the silty clay model (Figs. 10c and 11b–c). The Fuglen

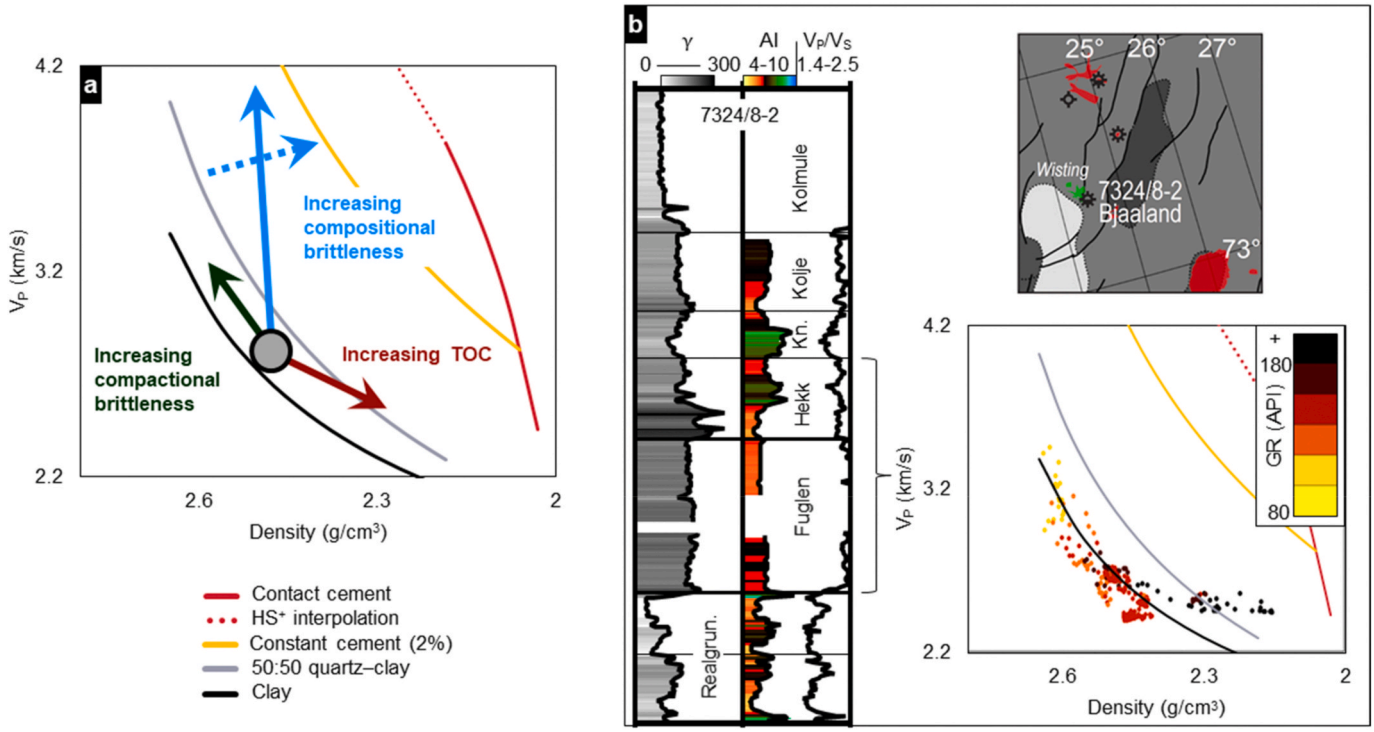

Fig. 13. (a) Schematic summary of different influences on a "shale" datapoint compared to rock physics template. (b) Caprock data from the Bjaaland well (7324/8–2) located close to proven discoveries in the Barents Sea (i.e., Wisting) show indications of excellent caprock quality.

and Hekkingen formation data from the Bjaaland well (7324/8–2) plot around the soft clay model, which we as previously mentioned would never expect a cemented claystone to follow, consistent with relatively shallow maximum burial depth (present burial 0.20–0.25 km BSF). Consequently, our interpretation is that the caprock here would likely be able to retain oil/gas, given the fulfillment of other trap requirements and availability of migrated hydrocarbons. Leakage through faults intersecting the reservoir structure is a more likely assertion to explain the absence of hydrocarbons. A horizontally drilled well in the nearby Wisting discovery lost drilling fluid when crossing such a fault plane, which supports the presence of conductive faults in the area (NPD, 2019). Faults in the Hoop Fault Complex intersecting the reservoir level were active as late as Aptian-Albian (Faleide et al., 2019). In a detailed study from the Hammerfest Basin, Edmundson et al. (2019) concluded that tectonic breaching, i.e., leakage along reactivated faults associated with Cenozoic uplift, is by far the most likely mechanism for hydrocarbon escape. Hermanrud et al. (2014) similarly proposed fault intersections as the main factor for hydrocarbon leakage after analyzing a wide range of structures in the Hammerfest Basin, finding that the only structure filled to capacity is one where no fault intersections cut through the top reservoir and caprock. Analogous observations were made in the study of a Northern North Sea gas discovery (well 35/10–2), where leakage again was attributed to fault intersections crosscutting the reservoir level, rather than seeing dispersed gas signatures across the structure that indicate a fractured seal. Pore pressure data and leak-off tests supported the interpretation that the associated caprock should not be hydrofractured (Teige and Hermanrud, 2004). In sum, fault intersection leakage seems to be a greater risk compared to cap rock efficiency and is well documented in the literature.

Another potential use of the template is assessment of heterogeneous reservoirs and potential flow barriers. Since the rock physics models appear generally consistent for any clay-quartz combination (cf. Figs. 5 and 6), they can be used inversely to relate low-permeability reservoir sections to velocity and density. This application is only valid for larger-scale lithology variations, as a thin clay-rich layer could be below seismic resolution, but still have great influence on reservoir connectivity, as exemplified by the capillary seal model in Fig. 7. Intrareservoir carbonate stringers or carbonate cemented sandstone layers can cause similar problems, but these are also typically much too thin for seismic characterization and are not evaluated in this study.

Thirdly, the presented trends can assist in unconventional shale characterization. One of the key properties that determine the potential of unconventional resources, for instance shale gas or other reservoirs that are too tight for conventional production, is the susceptibility to hydraulic fracture stimulation. In order to facilitate hydraulic fracturing, the target rock must be sufficiently brittle in relation to its mineralogical composition, porosity, and compaction. Another requirement for oil shale and shale gas reservoirs is a relatively high TOC content. By calibrating a template similar to Fig. 13a to relevant well log data, preferably coupled with an expression of production efficiency, we can use the same framework to evaluate both of these properties simultaneously. As an example, data from reservoir sections and nonreservoir sections in the Upper Jurassic Haynesville gas shale display average values within the bounds of our template (Lucier et al., 2011). An important additional consideration is introduced by thermal maturity and gas saturation, and the aforementioned applications therefore require calculation of gas-corrected velocities and density, e.g., as described by Lucier et al. (2011).

6. Conclusions

- We have presented a framework for interpreting composition and sealing efficiency of shales from acoustic properties, with supporting evidence from multiple wells in different regions of the Norwegian Continental Shelf.
- We demonstrate in ρ_b–V_P crossplots that the manner in which shale velocity changes compared to bulk density has significance, and can help distinguish changes related to mineralogical or organic matter content.
- Upper Jurassic seal quality is generally discarded as a significant risk factor for hydrocarbon exploration based on the investigated wells. The studied formations appear to have excellent caprock capabilities and ability to retain significant oil columns even in areas where the primary caprock is silty. Furthermore, clay-dominated Lower Cretaceous sequences overlie the immediate seal formations and serve as secondary caprocks. Additionally, intermediate gas accumulations have been discovered in areas of dramatic net uplift (~2 km). Consequently, uplift-generated conductive fracturing with a frequency sufficient to cause severe leakage of hydrocarbons seems unlikely.
- Poorly consolidated caprock shales may better maintain seal integrity after uplift due to more ductile behavior compared to cemented shales, given a relatively similar composition. We assume fracturing as a prerequisite for any leakage through the Upper Jurassic shale section, which may occur in well-consolidated, brittle shales due to the low permeability and high capillary entry pressure of clay-dominated rocks. Fault intersections should however be considered a greater risk in prospect evaluations.
- Differentiation between gas- and oil-sealing capabilities (which for a given seal also depends on the properties of the sealed fluid) does not seem plausible directly from elastic properties, which has implications for CO_2-storage seal assessments.

Declaration of competing interest

The authors declare that they have no known competing financial interests or personal relationships that could have appeared to influence the work reported in this paper.

CRediT authorship contribution statement

Jørgen André Hansen: Conceptualization, Methodology, Formal analysis, Writing - original draft, Writing - review & editing, Visualization. **Nazmul Haque Mondol:** Conceptualization, Writing - review & editing, Supervision, Project administration, Funding acquisition. **Filippos Tsikalas:** Writing - review & editing, Supervision, Funding acquisition. **Jan Inge Faleide:** Writing - review & editing, Supervision, Visualization.

Acknowledgements

This research is part of the “ReSource – Quantitative analysis of reservoir, source and cap rocks of the Central North Sea” project. We are grateful to Vår Energi (previously Eni Norge) for funding the PhD program of Jørgen A. Hansen and for providing seismic data. All other data are courtesy of the Norwegian Petroleum Directorate (NPD) through the DISKOS national data repository (https://www.npd.no/en/diskos/). Jamil Rahman (UiO) is acknowledged for SEM and XRD analysis, and Jens Jahren (UiO) for discussions and helpful input. Academic software licences are provided by CGG for Hampson-Russell software, Lloyd’s register for Interactive Petrophysics, and Schlumberger for Petrel.

Appendix A. Supplementary data

Supplementary data to this article can be found online at https://doi.org/10.1016/j.marpetgeo.2020.104603.

References

Aplin, A.C., Moore, J.K.S., 2016. Observations of pore systems of natural siliciclastic mudstones. Clay Miner. Soc. Workshop Lect. Ser. 21, 33–44. https://doi.org/10.1346/CMS-WLS-21.3.

Asquith, G., Krygowski, D.A., 2004. Basic well log analysis In: AAPG Methods in Exploration, second ed., vol. 16. The American Association of Petroleum Geologists, Tulsa, OK, U.S.

Avseth, P., Mukerji, T., Mavko, G., 2005. Quantitative Seismic Interpretation: Applying Rock Physics Tools to Reduce Interpretation Risk. Cambridge University Press, Cambridge, U.K. https://doi.org/10.1017/CBO9780511600074.

Baig, I., Faleide, J.I., Jahren, J., Mondol, N.H., 2016. Cenozoic exhumation on the southwestern Barents Shelf: estimates and uncertainties constrained from compaction and thermal maturity analyses. Mar. Petrol. Geol. 73, 105–130. https://doi.org/10.1016/j.marpetgeo.2016.02.024.

Baig, I., Faleide, J.I., Mondol, N.H., Jahren, J., 2019. Burial and exhumation history controls on shale compaction and thermal maturity along the Norwegian North Sea basin margin areas. Mar. Petrol. Geol. 104, 61–85. https://doi.org/10.1016/j.marpetgeo.2019.03.010.

Batzle, M., Wang, Z., 1992. Seismic properties of pore fluids. Geophysics 57 (11), 1396–1408. https://doi.org/10.1190/1.1443207.

Birchall, T., Senger, K., Olaussen, S., 2018. Subnormal pressure regimes of the Northern Barents Shelf: causes and implications for hydrocarbon exploration. In: 80th EAGE Conference & Exhibition Conference Proceedings. European Association of Geoscientists & Engineers, Copenhagen, Denmark, p. 5. https://doi.org/10.3997/2214-4609.201800913.

Bjørlykke, K., 2015. Petroleum migration. In: Bjørlykke, K. (Ed.), Petroleum Geoscience. From Sedimentary Environments to Rock Physics, second ed. Springer-Verlag Berlin Heidelberg, pp. 373–384. https://doi.org/10.1007/978-3-642-34132-8.

Bredesen, K., Avseth, P., Johansen, T.A., Olstad, R., 2019. Rock physics modelling based on depositional and burial history of Barents Sea sandstones. Geophys. Prospect. 67, 825–842.

Buia, M., Cirone, C., Leutscher, J., Tarran, S., Webb, B., 2010. Multi-azimuth 3D survey in the Barents Sea. First Break 28, 65–69.

Carcione, J.M., Avseth, P., 2015. Rock-physics templates for clay-rich source rocks. Geophysics 80 (5), D481–D500. https://doi.org/10.1190/GEO2014-0510.1.

Dalland, A., Worsley, D., Ofstad, K., 1988. A lithostratigraphic scheme for the Mesozoic and Cenozoic succession offshore mid- and northern Norway. NPD Bull. 4, 1–65.

Dewhurst, D.N., Yang, Y., Aplin, A.C., 1999. Permeability and fluid flow in natural mudstones. In: Aplin, A.C., Fleet, A.J., Macquaker, J.H.S. (Eds.), Muds and Mudstones: Physical and Fluid Flow Properties, vol. 158. The Geological Society of London, London, U.K, pp. 23–43. https://doi.org/10.1144/GSL.SP.1999.158.01.03.

Doré, A.G., Vollset, J., Hamar, G.P., 1985. Correlation of the offshore sequences referred to the Kimmeridge Clay Formation - relevance to the Norwegian sector. In: Thomas, B.M., Doré, A.G., Eggen, S., Home, P.C., Larsen, R.M. (Eds.), Petroleum Geochemistry in Exploration of the Norwegian Shelf, vol. 1. Springer, Dordrecht, Netherlands, pp. 27–37.

Doré, A.G., Corcoran, D.V., Scotchman, I.C., 2002. Prediction of the hydrocarbon system in exhumed basins, and application to the NW European margin. In: Doré, A.G., Cartwright, J.A., Stoker, M.S., Turner, J.P., White, N. (Eds.), Exhumation of the North Atlantic Margin: Timing, Mechanisms and Implications for Petroleum Exploration, vol. 196. The Geological Society, London, U.K, pp. 401–429. https://doi.org/10.1144/GSL.SP.2002.196.01.21.

Doveton, J.H., 1994. Geological Log Interpretation. *SEPM Short Course Notes* (29. U.S.: Society for Sedimentary Geology, Tulsa, OK. https://doi.org/10.2110/scn.94.29.

Downey, M.W., 1984. Evaluating seals for hydrocarbon accumulations. AAPG (Am. Assoc. Pet. Geol.) Bull. 68 (11), 1752–1763. https://doi.org/10.1306/AD461994-16F7-11D7-8645000102C1865D.

Dvorkin, J., Nur, A., 1996. Elasticity of high-porosity sandstones: theory for two North Sea data sets. Geophysics 61 (5), 1363–1370. https://doi.org/10.1190/1.1444059.

Edmundson, I., Rotevatn, A., Davies, R., Yielding, G., Broberg, K., 2019. Key Controls on Hydrocarbon Retention and Leakage from Structural Traps in the Hammerfest Basin, SW Barents Sea: Implications for Prospect Analysis and Risk Assessment. *Petroleum Geoscience*. Advance online publication. https://doi.org/10.1144/petgeo2019-094.

Faleide, J.I., Tsikalas, F., Breivik, A.J., Mjelde, R., Ritzmann, O., Engen, Ø., et al., 2008. Structure and evolution of the continental margin off Norway and the Barents Sea. Episodes 31 (1), 82–91. https://doi.org/10.18814/epiiugs/2008/v31i1/012.

Faleide, J.I., Bjørlykke, K., Gabrielsen, R.H., 2015. Geology of the Norwegian continental shelf. In: Bjørlykke, K. (Ed.), Petroleum Geoscience. From Sedimentary Environments to Rock Physics, second ed. Springer-Verlag Berlin Heidelberg, pp. 603–638. https://doi.org/10.1007/978-3-642-34132-8.

Faleide, T.S., Midtkandal, I., Planke, S., Corseri, R., Faleide, J.I., Serck, C.S., Nystuen, J. P., 2019. Characterisation and development of Early Cretaceous shelf platform deposition and faulting in the Hoop area, southwestern Barents Sea—constrained by high-resolution seismic data. Norw. J. Geol. 99 (3), 1–20. https://doi.org/10.17850/njg99-3-7.

Gabrielsen, R.H., Kløvjan, O.S., 1997. Late Jurassic-early Cretaceous caprocks of the southwestern Barents Sea: fracture systems and rock mechanical properties. In: Møller-Pedersen, P., Koestler, A.G. (Eds.), Hydrocarbon Seals: Importance for Exploration and Production. Norwegian Petroleum Society Special Publication, vol. 7. Elsevier, Singapore, pp. 73–89. https://doi.org/10.1016/S0928-8937(97)80008-2.

Goodway, B., Chen, T., Downton, J., 1997. Improved AVO Fluid Detection and Lithology Discrimination Using Lamé Petrophysical Parameters; "λρ", "μρ", & "λ/μ Fluid Stack", from P and S Inversions. *SEG Technical Program Expanded Abstracts 1997*. Society of Exploration Geophysicists, pp. 183–186. https://doi.org/10.1190/1.1885795.

Gray, L., Anderson, P., Logel, J., Delbecq, F., Schmidt, D., Schmid, R., 2012. Estimation of stress and geomechanical properties using 3D seismic data. First Break 30 (3), 59–68. https://doi.org/10.3997/1365-2397.2011042.

Guo, Z., Li, X.-Y., Liu, C., Feng, X., Shen, Y., 2013. A shale rock physics model for analysis of brittleness index, mineralogy and porosity in the Barnett Shale. J. Geophys. Eng. 10, 1–10. https://doi.org/10.1088/1742-2132/10/2/025006.

Hall, D.M., Duff, B.A., Elias, M., Gytri, S.R., 1997. Pre-cretaceous top-seal integrity in the greater Ekofisk area. In: Møller-Pedersen, P., Koestler, A.G. (Eds.), Hydrocarbon Seals: Importance for Exploration and Production. Norwegian Petroleum Society Special Publication, vol. 7. Elsevier, Singapore, pp. 231–242. https://doi.org/10.1016/S0928-8937(97)80019-7.

Hansen, J.A., Yenwongfai, H.D., Fawad, M., Mondol, N.H., 2017. Estimating exhumation using experimental compaction trends and rock physics relations, with continuation into analysis of source and reservoir rocks: central North Sea, offshore Norway. In: SEG Technical Program Expanded Abstracts, vol. 2017. Society of Exploration Geophysicists, pp. 3971–3975. https://doi.org/10.1190/segam2017-17783053.1.

Hansen, J.A., Mondol, N.H., Fawad, M., 2019. Organic content and maturation effects on elastic properties of source rock shales in the Central North Sea. Interpretation 7 (2), T477–T497. https://doi.org/10.1190/INT-2018-0105.1.

Hansen, J.A., Mondol, N.H., Jahren, J., Tsikalas, F., 2020. Reservoir assessment of middle jurassic sandstone-dominated formations in the Egersund Basin and ling depression, eastern Central North sea. Mar. Petrol. Geol. 111, 529–543. https://doi.org/10.1016/j.marpetgeo.2019.08.044.

Henriksen, E., Bjørnseth, H.M., Hals, T.K., Heide, T., Kiryukhina, T., Kløvjan, O.S., et al., 2011. Uplift and erosion of the greater Barents Sea: impact on prospectivity and petroleum systems. In: Spencer, A.M., Embry, A.F., Gautier, D.L., Stoupakova, A.V., Sørensen, K. (Eds.), Arctic Petroleum Geology, vol. 35. Geological Society, Memoirs, London, pp. 271–281. https://doi.org/10.1144/M35.17.

Hermanrud, C., Eggen, S., Jacobsen, T., Carlsen, E.M., Pallesen, S., 1990. On the accuracy of modelling hydrocarbon generation and migration: the Egersund Basin oil find, Norway. Org. Geochem. 16 (1–3), 389–399. https://doi.org/10.1016/0146-6380(90)90056-6.

Hermanrud, C., Halkjelsvik, M.E., Kristiansen, K., Bernal, A., Strömbäck, A.C., 2014. Petroleum column-height controls in the western Hammerfest Basin, Barents Sea. Petrol. Geosci. 20, 227–240. https://doi.org/10.1144/petgeo2013-041.

Holt, R.M., Fjær, E., Stenebråten, J.F., Nes, O.-M., 2015. Brittleness of shales: relevance to borehole collapse and hydraulic fracturing. J. Petrol. Sci. Eng. 131, 200–209.

Ingram, G.M., Urai, J.L., Naylor, M.A., 1997. Sealing processes and top seal assessment. In: Møller-Pedersen, P., Koestler, A.G. (Eds.), Hydrocarbon Seals: Importance for Exploration and Production. Norwegian Petroleum Society Special Publication, vol. 7. Elsevier, Singapore, pp. 165–174. https://doi.org/10.1016/S0928-8937(97)80014-8.

Kalani, M., Jahren, J., Mondol, N.H., Faleide, J.I., 2015. Petrophysical implications of source rock microfracturing. Int. J. Coal Geol. 143, 43–67. https://doi.org/10.1016/j.coal.2015.03.009.

Lerch, B., Karlsen, D.A., Abay, T.B., Duggan, D., Seland, R., Backer-Owe, K., 2016. Regional petroleum alteration trends in Barents Sea oils and condensates as a clue to migration regimes and processes. AAPG (Am. Assoc. Pet. Geol.) Bull. 100 (2), 165–190. https://doi.org/10.1306/08101514152.

Løseth, H., Lippard, S.J., Sættem, J., Fanavoll, S., Fjerdingstad, V., Leith, T.L., et al., 1992. Cenozoic uplift and erosion of the Barents Sea — evidence from the svalis dome area. In: Vorren, T.O., Bergsager, E., Dahl-Stamnes, Ø.A., Holter, E., Johansen, B., Lie, E., Lund, T.B. (Eds.), Arctic Geology and Petroleum Potential. Norwegian Petroleum Society Special Publication, vol. 2. Elsevier, Amsterdam, Netherlands, pp. 643–664. https://doi.org/10.1016/B978-0-444-88943-0.50042-3.

Løseth, H., Gading, M., Wensaas, L., 2009. Hydrocarbon leakage interpreted on seismic data. Mar. Petrol. Geol. 26 (7), 1304–1319. https://doi.org/10.1016/j.marpetgeo.2008.09.008.

Lucier, A.M., Hofmann, R., Bryndzia, L.T., 2011. Evaluation of variable gas saturation on acoustic log data from the Haynesville Shale gas play, NW Louisiana, USA. Lead. Edge 30 (3), 300–311. https://doi.org/10.1190/1.3567261.

Makurat, A., Tørudbakken, B., Monsen, K., Rawlings, C., 1992. Cenezoic uplift and caprock seal in the Barents Sea: fracture modelling and seal risk evaluation - SPE 24740. In: 67th Annual Technical Conference and Exhibition of the SPE Proceedings. Society of Petroleum Engineers, Washington, DC, U.S, pp. 821–830. https://doi.org/10.2118/24740-MS.

Mavko, G., Mukerji, T., Dvorkin, J., 2009. The Rock Physics Handbook: Tools for Seismic Analysis of Porous Media, second ed. Cambridge University Press, Cambride, U.K. https://doi.org/10.1017/CBO9780511626753.

Mulrooney, M.J., Leutscher, J., Braathen, A., 2017. A 3D structural analysis of the Goliat field, Barents Sea, Norway. Mar. Petrol. Geol. 86, 192–212. https://doi.org/10.1016/j.marpetgeo.2017.05.038.

Mulrooney, M.J., Rismyhr, B., Yenwongfai, H.D., Leutscher, J., Olaussen, S., Braathen, A., 2018. Impacts of small-scale faults on continental to coastal plain deposition: evidence from the Realgrunnen Subgroup in the Goliat field, southwest Barents Sea, Norway. Mar. Petrol. Geol. 95, 276–302. https://doi.org/10.1016/j.marpetgeo.2018.04.023.

Nooraiepour, M., Mondol, N.H., Hellevang, H., Bjørlykke, K., 2017. Experimental mechanical compaction of reconstituted shale and mudstone aggregates: investigation of petrophysical and acoustic properties of SW Barents Sea cap rock sequences. Mar. Petrol. Geol. 80, 265–292. https://doi.org/10.1016/j.marpetgeo.2016.12.003.

NPD, 2019. Norwegian Petroleum Directorate FactPages. http://factpages.npd.no/factpages/.

Ødegaard, E., Avseth, P., 2004. Well log and seismic data analysis using rock physics templates. First Break 23, 37–43. https://doi.org/10.3997/1365-2397.2004017.

Ohm, S.E., Karlsen, D.A., Austin, T.J.F., 2008. Geochemically driven exploration models in uplifted areas: example from the Norwegian Barents Sea. AAPG (Am. Assoc. Pet. Geol.) Bull. 92 (9), 1191–1223. https://doi.org/10.1306/06180808028.

Olstad, R., Bjørlykke, K., Karlsen, D.A., 1997. Pore water flow and petroleum migration in the Smørbukk field area, offshore mid-Norway. In: Møller-Pedersen, P., Koestler, A.G. (Eds.), Hydrocarbon Seals: Importance for Exploration and Production. Norwegian Petroleum Society Special Publication, vol. 7. Elsevier, Singapore, pp. 201–217. https://doi.org/10.1016/S0928-8937(97)80017-3.

Perez, R., Marfurt, K., 2014. Mineralogy-based brittleness prediction from surface seismic data: application to the Barnett Shale. Interpretation 2 (4), T255–T271. https://doi.org/10.1190/INT-2013-0161.1.

Purcell, W.R., 1949. Capillary pressure – their measurements using mercury and the calculation of permeability therefrom. AIME Petrol. Trans. 186, 39–48.

Ritter, U., 1988. Modelling of hydrocarbon generation patterns in the Egersund Sub-basin, North Sea. Adv. Org. Geochem. 13 (1–3), 165–174. https://doi.org/10.1016/0146-6380(88)90036-8.

Sales, J.K., 1993. Closure vs. seal capacity - a fundamental control on the distribution of oil and gas. In: Doré, A.G., Augustson, J.H., Hermanrud, C., Steward, D.J., Sylta, Ø. (Eds.), Basin Modeling: Advances and Application. Norwegian Petroleum Society Special Publication, vol. 3. Elsevier, Amsterdam, Netherlands, pp. 399–414.

Schowalter, T.T., 1979. Mechanics of secondary hydrocarbon migration and entrapment. AAPG (Am. Assoc. Pet. Geol.) Bull. 633 (5), 723–760. https://doi.org/10.1306/2F9182CA-16CE-11D7-8645000102C1865D.

Skurtveit, E., Grande, L., Ogebule, O.Y., Gabrielsen, R.H., Faleide, J.I., Mondol, N.H., et al., 2015. Mechanical testing and sealing capacity of the upper jurassic Draupne formation, North Sea. In: 49th US Rock Mechanics/Geomechanics Symposium Expanded Abstracts ARMA-2015-331. American Rock Mechanics Association, San Francisco, California, U.S., p. 8

Teige, G.M.G., Hermanrud, C., 2004. Seismic characteristics of fluid leakage from an underfilled and overpressured Jurassic fault trap in the Norwegian North Sea. Petrol. Geosci. 10, 35–42. https://doi.org/10.1144/1354-079302-548.

Teige, G.M.G., Hermanrud, C., Thomas, W.H., Wilson, O.B., Bolås, H.M.N., 2005. Capillary resistance and trapping of hydrocarbons: a laboratory experiment. Petrol. Geosci. 11, 125–129. https://doi.org/10.1144/1354-079304-609.

Thyberg, B., Jahren, J., Winje, T., Bjørlykke, K., Faleide, J.I., 2009. From mud to shale: rock stiffening by micro-quartz cementation. First Break 27, 53–59.

Tosaya, C.A., 1982. *Acoustical Properties of Clay-Bearing Rocks*, (Doctoral Dissertation). Stanford University, Stanford, CA, U.S.. Retrieved from Pangea. https://pangea.stanford.edu/departments/geophysics/dropbox/SRB/public/docs/theses/SRB_015_JUN82_Tosaya.pdf

Tsikalas, F., Uncini, G., Mavilla, N., Staine, I., Casaglia, F., Leutscher, J., et al., 2017. Goliat discovery – a knowledge-based approach, persistence and the first commercial oil development in the Norwegian arctic. AAPG datapages/search and discovery article #20415. In: Paper Presented at AAPG/SEG International Conference and Exhibition, London, England.

Vernik, L., 2016. Seismic Petrophysics in Quantitative Interpretation. Investigations in Geophysics Series, vol. 18. Society of Exploration Geophysicists, Tulsa, OK, U.S.

Vollset, J., Doré, A.G., 1984. A revised triassic and jurassic lithostratigraphic nomenclature for the Norwegian North Sea. NPD Bull. 3, 1–53.

Yenwongfai, H.D., Mondol, N.H., Faleide, J.I., Lecomte, I., 2017. Prestack simultaneous inversion to predict lithology and pore fluid in the Realgrunnen Subgroup of the Goliat Field, southwestern Barents Sea. Interpretation 5 (2), SE75–SE96. https://doi.org/10.1190/INT-2016-0109.1.

Yenwongfai, H.D., Mondol, N.H., Lecomte, I., Faleide, J.I., Leutscher, J., 2018. Integrating facies-based Bayesian inversion and supervised machine learning for petro-facies characterization in the Snadd Formation of the Goliat Field, south-western Barents Sea. Geophys. Prospect. 67 (4), 1020–1039. https://doi.org/10.1111/1365-2478.12654.

Zadeh, M.K., Mondol, N.H., Jahren, J., 2017. Velocity anisotropy of upper jurassic organic-rich shales, Norwegian continental shelf. Geophysics 82 (2), C61–C75. https://doi.org/10.1190/geo2016-0035.1.

Zhao, L., Qin, X., Han, D.-H., Geng, J., Yang, Z., Cao, H., 2016. Rock-physics modeling for the elastic properties of organic shale at different maturity stages. Geophysics 81 (5), D527–D541. https://doi.org/10.1190/geo2015-0713.1.